Sedimentary processes and palaeoenvironments from La Combette sequence (southeastern France)

Mologni, Carlo; Purdue, Louise; Audiard, Benjamin; Dubar, Michel; Kreutzer, Sebastian; Texier, Pierre-jean

Published in:
Palaeogeography, Palaeoclimatology, Palaeoecology

DOI:
10.1016/j.palaeo.2021.110503

Publication date:
2021

Citation for published version (APA):
Mologni, C., Purdue, L., Audiard, B., Dubar, M., Kreutzer, S., & Texier, P. (2021). Sedimentary processes and palaeoenvironments from La Combette sequence (southeastern France): Climatic insights on the Last Interglacial/Glacial transition. *Palaeogeography, Palaeoclimatology, Palaeoecology*, *576*, [110503]. https://doi.org/10.1016/j.palaeo.2021.110503

Sedimentary processes and palaeoenvironments from La Combette sequence (southeastern France): climatic insights on the Last Interglacial/Glacial transition

Carlo Mologni [a, b *], Louise Purdue [b], Benjamin Audiard [b], Michel Dubar [b], Sebastian Kreutzer [c,d], Pierre-Jean Texier [e]

[a] Université Côte d'Azur, CNRS, Observatoire de la Côte d'Azur, IRD, Géoazur, 250 rue Albert Einstein, 06905 Sophia Antipolis, France

[b] Université Côte d’Azur, CNRS, CEPAM-UMR7264, 24 avenue des Diables Bleus 06357, Nice, France.

[c] Geography & Earth Sciences, Aberystwyth University, SY23 3DB, Wales, United Kingdom

[d] Université Bordeaux Montaigne, CNRS, IRAMAT-CRP2A-UMR5060, Maison de l’Archéologie, Esplanade des Antilles, 33607 Pessac Cedex, France

[e] Aix Marseille Univ, CNRS, Minist Culture, LAMPEA, UMR 72-69, 5 rue du château de l’horloge, 13094 Aix-en-Provence, France

[*]corresponding author: Carlo Mologni: mologni@geoazur.unice.fr

Louise Purdue (louise.purdue@cepam.cnrs.fr)

Benjamin Audiard (bejamin.audiard@cepam.cnrs.fr)

Michel Dubar (michel.dubar@cepam.cnrs.fr)

Sebastian Kreutzer (sebastian.kreutzer@aber.ac.uk)

Pierre-Jean Texier (pj.texier@gmail.com)

Accepted manuscript version prior to proof-reading.
For the published version see: https://doi.org/10.1016/j.palaeo.2021.110503

Abstract

During the Last Interglacial-Early Glacial transition (MIS5-MIS4; ~73 ka), substantial hydroclimatic changes affected morphogenetic processes, landform dynamics, and ecosystem variability over the Mediterranean sub-alpine valleys. This transition is mainly preserved in the northern Mediterranean region in continuous marine, lacustrine, and peat bog archives. To understand better local-to-regional hydro-sedimentary processes, their climatic significance, and their direct impact on prehistoric settlements, this manuscript reinvestigates a known continental sedimentary record with revised methods. The Middle Palaeolithic site of La Combette in the western Provence region (southeastern France) presents a thick sedimentary sequence key for studying environmental changes from the MIS5 to the MIS3. A review of previous studies with the integration of new micromorphological, sedimentological, physicochemical, malacological, and luminescence ages allows us to characterize the sedimentary processes and environmental patterns during this major climatic transition. Alternating warm and cold conditions and shifting vegetation patterns reflect the strong environmental instability of the end of the Last Interglacial Period. The emergence of a steppe-like ecology dominated by cryo-turbated loess deposition marks the beginning of the Early Würmian Glacial period (MIS4-MIS3; ~73 ka to ~50 ka), contemporaneous with the last Neanderthal occupation at La Combette rock shelter. Comparisons with regional palaeoclimatic data allow us to detail local climatic settings and provide evidence of divergences with larger-scale quantitative reconstructions during a period of significant environmental and socio-cultural shifts.

Keywords: MIS 5-3; Multiproxy; Neanderthal; Loess; Micromorphology; Chronology

1 - Introduction

Confronting global climate models with regional environmental trends is essential to understand the evolution of palaeolandscapes and their impact on the development of ecosystems and prehistoric population dynamics. Interglacial-glacial transitions represent sensitive periods for the comprehension of landforms' reactivity to global hydroclimatic variations (Klotz et al., 2004) in relation to prehistoric peopling. In particular, the Last

Interglacial-Glacial transition (LI-G; MIS5-MIS4-MIS3, ~90 – ~50 ka) shows several sub-stage oscillations, sometimes abrupt (Reille et al., 1992; Salonen et al., 2018), mainly towards the onset of glacial Würmian conditions.

In southeastern France, only a few continuous sedimentary records have recorded the LI-G climatic transition. One submarine core covering this cycle was extracted from the deep Rhône delta (Gulf of Lion, MD99-2348 core; Sierro et al., 2009; Fig. 1). It reveals temperate conditions and high fluvial activity during the interglacial MIS 5, followed by reduced hydrological activity and a shift towards cooler and drier conditions during the MIS5 – MIS4 transition. Further north, in the septentrional Rhône basin, the palynological study of the peats sequences of Les Echets (Beaulieu and Reille, 1984; de Beaulieu and Reille, 1989) and La Grande Pile (Fauquette et al., 1999; Helmens, 2014; Seret et al., 1990; Woillard and Mook, 1982; Fig. 1) indicate a substantial reduction of rainfall and temperatures (Fauquette et al., 1999) with the spread of steppe taxa. However, the beginning MIS4 seems to be interspersed by slight warmer oscillations, attesting a period of progressive environmental stabilisation thought the glacial conditions, definitely installed around ~60 ka (Fauquette et al., 1999; Helmens, 2014). A recent study on a loess-palaeosol sequence in the Lower Rhône valley provides the first robust loess chronosequence from the Early Würmian glaciation in the south of France confirming this transition (Bosq et al., 2020b). However, most sedimentary records in southeastern France covering this period and linked to Neanderthal occupations (archaeological stratigraphy) are non-continuous and incomplete, adding a considerable uncertainty to the environmental interpretations (Fig. 1). For instance, this is the case at Bau de l'Aubesier (MIS5 or 6; Lebel and Trinkaus, 2002), the Grand abri aux Puces (MIS5e; Slimak et al., 2010), the Baume Bonne (from MIS 10, lack of MIS 5-4; Gagnepain and Gaillard, 2003), Les Auzières 2 (MIS4; Marchal et al.,

Accepted manuscript version prior to proof-reading.
For the published version see: https://doi.org/10.1016/j.palaeo.2021.110503

2009), and the Payre (MIS6-MIS5; Moncel et al., 2008). Apart from a few well-dated sites such as Moula-Guercy (Saos et al., 2014; Willmes et al., 2016), the Baume Flandin, the Pêcheurs, and the Maras rock shelters (Moncel et al., 2010), most of the excavated sequences lack absolute dating, e.g., Baume des Peyrards (de Lumley, 1969, 1957), Adaouste Cave (Conrad and Onoratini, 1997; Defleur et al., 1994), La Verrerie (Crégut-Bonnoure, 2002). Understanding the regional-to-local environmental patterns of prehistoric occupations during prominent climatic disruptions is fundamental for interpreting archaeological records. Moreover, most of these archaeological sites need to high-resolution studies, which are the key to decipher this complex climatic transition. In the Mediterranean region, cave and rock shelter sediments have the potential to record abrupt climatic changes, in particular, if investigated by a microstratigraphic perspective (Courty and Vallverdu, 2001; Macklin and Woodward, 2009; Woodward et al., 2001).

With the aim to provide new data and fuel the debate on the palaeoenvironmental background of the LI-G Neanderthal occupations, we reinvestigated the continental sequence of the La Combette rock shelter through a new chronology (Kreutzer et al., 2021). Based on a review of previous palynological (López-Sáez et al., 1998) and charcoal analyses (Audiard et al., 2019; Théry-Parisot and Texier, 2006) and the data improvement with new micromorphological, sedimentological, physicochemical, and malacological analyses, we propose a detailed palaeoenvironmental evolution of the La Combette sequence in connection with LI-G broader hydro-climatic shifts. Our results combine previous regional records in order to identify and discuss the local and/or regional impact of climatic change on the local landscape dynamics, adding to our comprehension of the complex environmental nuances of the Last Interglacial – Glacial transition in the Mediterranean.

Accepted manuscript version prior to proof-reading.
For the published version see: https://doi.org/10.1016/j.palaeo.2021.110503

2 – Regional settings and site description

At an elevation of 327 m a.s.l., the rock shelter is located along the La Combette stream, in the Aigue Brun valley, a tributary of the Durance river, part of the Rhône river hydrological system (Figs. 1, 2a). The stream originates locally from the Luberon Massif, a few kilometers from the shelter, which borders the northern sub-alpine domain of the Vaucluse Mountains and the southern Provençal-Littoral domain. The river course crosses Urgonian (Lower Cretaceous), Oligocene, and Miocene molasses calcareous rocks, which compose the rock shelter. Due to the N-S mistral wind regime (16 m/s for >100 d/y; Jacq et al., 2005), the area is constituted of numerous ancient aeolian landforms like sand wedges, ventifacts, loess deposits, and freeze/thaw structures (Bertran et al., 2016; Bosq et al., 2020b, 2020a, 2018; Fig. 1). The lithostratigraphic sequence of La Combette belongs to these periglacial morphosedimentary features (Fig. 1, 2; Buoncristiani and Campy, 2011; Cossart et al., 2011, 2008; Tiercelin, 1977).

Multidisciplinary studies in La Combette rock shelter were conducted between the 1990 to 2002. Combined techno-functional (lithic technology and traceology), archaeo-petrographic, anthracological, palynological, archaeozoological, and thermally stimulated luminescence (TL) analyses (Lemorini, 2000; López-Sáez et al., 1998; Texier et al., 2003; Théry-Parisot and Texier, 2006; Wilson et al., 2018) provided unique knowledge on Neanderthal subsistence strategies in southeastern France (Daujeard et al., 2012; Théry-Parisot and Texier, 2006; Wilson et al., 2018). However, a detailed sedimentological and geochronological study of the sequence, as well as their palaeoclimatic relevance, had never been attempted until today.

3 - Material and methods

3.1 – Field methods and sampling strategy

During the excavation in the 1990s, two prominent sedimentary ensembles (Upper and Lower) with eight archaeological levels were differentiated (A to H; Texier et al., 2003). In 2019, a field campaign allowed us to examine more precisely this sedimentary sequence and define 19 new sedimentary units (SU; Fig. 3) based on texture, structure, color, sorting, boundaries, and inclusions (ecological, sedimentary, or anthropic).

The new stratigraphic layers were sampled for magnetic susceptibility, sedimentological, pedological and palaeoecological studies. The magnetic susceptibility (SI) was measured in the field every 5 cm with a Bartington MS2 Instrument (10-5 SI), except on gravelly deposits to avoid magnetic anomalies. Thin section samples were carved in the lower and upper ensemble from the eastern section of La Combette (Fig. 3). Bulk sediments were sampled for sedimentary analyses (grain size, heavy minerals, $CaCO_3$ content) next to the micromorphological samples (Fig. 3). A total of 17 micromorphological blocks and 48 bulk sediments were sampled.

From the northern section of La Combette, 22 bulk sediment samples were collected (10 l sediment each sample) along with the Lower and Upper ensembles for malacological study. Malacofauna samples were sieved with 0.8 mm sieves, manually sorted, and identified under a binocular microscope.

To refine the geochronological framework and test whether the Lower Ensemble might belong to the MIS 6/7 (a hypothesis put forward by Walther, 1995), the sedimentary section was re-investigated by Kreutzer et al., 2021. Six new samples were taken from the main archaeological levels for luminescence dating (Table 1).

3.2 – Laboratory methods

3.2.1 – Micromorphology

Soil thin sections were prepared following the standard procedure described in (Guillore, 1980). Seventeen thin sections were studied under a polarizing microscope Zeiss Axioskop 40 Pol/ 40 A Pol at a magnification between 25x and 1000x using plane-polarized (PPL), crossed-polarized (XPL), and fluorescence light (UV). Thin sections are described following the guidelines proposed by Bullock (1985) and Stoops (2003).

3.2.2 –Physicochemical analysis

Grain size analysis was performed on a Beckman Coulter LS200 laser diffraction particle size analyzer. Samples were deflocculated with sodium hexametaphosphate solution and decarbonized with HCl (1 mol; Konert and Vandenberghe, 1997). Given the limited amount of organic material (cf. micromorphological observations; section 4.2), organic components were not destroyed. Furthermore, to ensure that authigenic carbonates did not bias the particle size signal, grain size measurements were performed on both carbonated and decarbonated samples.

The $CaCO_3$ concentration in sediments was determined using a Bernard calcimeter (Cailleux and Tricart, 1964). The samples were sieved at 2 mm, crushed, weighed, and dissolved

Accepted manuscript version prior to proof-reading.
For the published version see: https://doi.org/10.1016/j.palaeo.2021.110503

in an HCl ½ solution. The CO_2 volume was measured, and the calcimeter was calibrated by measuring the CO_2 volume of pure calcium carbonate.

3.2.3 – Heavy-mineral analysis

Sample preparation for heavy-mineral determination followed the procedure described in Cailleux and Tricart (1964) and Parfenoff et al. (1970). Because of the silt and fine sand texture of the deposits, we analyzed the 200-40 µm fraction. Samples (100 g) were decarbonized in HCl at 20°C and 80°C, while heavy minerals were separated by immersion and decantation in a tribromomethane solution ($CHBr_3$, 2.89 g/cm^3) and fixed on non-polished thin sections with a natural isotropic resin. Mineral identification was performed under a polarizing microscope Zeiss Axioskop 40 Pol/ 40 A Pol on samples of 150 grains per section. The local mineral assemblage was identified based on the heavy mineral extraction of molassic parent rock material from the rock shelter vault and the bedrock of Aigue Brun canyon.

3.2.4 – Luminescence dating details

For luminescence dating, Kreutzer et al. (2021) extracted the fine grain (4–11 µm) quartz and polymineral fraction following routine luminescence sample preparation methods (Preusser et al., 2008). The quartz fraction was measured with optically stimulated luminescence (OSL; Huntley et al., 1985) applying the single-aliquot regenerative- (SAR, Murray and Wintle, 2000) dose protocol. The polymineral fraction was measured with infrared stimulated luminescence (IRSL; Hütt et al., 1986), applying the post-IR IRSL protocol at 225 ˚C (Buylaert et al., 2009; Thomsen et al., 2008). Measurements were carried out on a Freiberg Instrument *lexsyg SMART* OSL/TL reader (Richter et al., 2015). Dose rates were measured *in* *situ* with passive carbon-doped dosimeters (for the procedure, see Kreutzer et al., 2018) in conjunction with high-resolution gamma-ray spectrometry. The ages results, corresponding to the archaeological layers, are presented in Table 1.

4 – Results

4.1 – Stratigraphy and geochronology

Based on the redefinition of the stratigraphy in 2019, we kept the initial lower and upper ensemble, but the former was divided into three sub-ensembles identified by the roman numbers I, II, III (Fig. 2b, 3; see Sup. Mat. Table A.1 for detailed SU pedo-sedimentary description).

From the bottom to the top, the Sub-ensemble-I is composed of three colluvial stratigraphic units (SU19-18-17) characterized by a) poor textural variability, mainly weakly-sorted sandy silts with gravel inclusions, b) absence of layering, c) high density of archaeological remains (layer F/G; Texier et al., 2003). Traces of vault collapse prior to the shelter sedimentary fill were observed. One luminescence date was obtained in stratum 17 and provided 71.9 ± 5.5 ka (BDX16816; Fig. 3b, Table 1) corresponding to the top of the archaeological layer F/G described in Texier et al., (2003).

Sub-ensemble-II.a (SU16, 15, 14, 13, 12, 11, 10) is characterized by fine alternating sands and silts typical of a layered rhythmic deposition. Following an erosional contact, Sub-ensemble-II.b (9, 8) is a coarser and massive deposit composed of sub-angular clasts in a sandy-silty matrix. Numerous Mousterian artifacts and combustion structures were discovered in SU8 corresponding to archaeological layer E (Texier et al. 2003), which was dated from 80.1 ± 6.4 ka (BDX16815; Fig. 3b, Table 1)

Sub-ensemble-III (SU7-6; Fig. 3b) comprises gravels and molassic blocs (10 cm to 50 cm) in a coarse-sandy matrix, mainly located in the southern part of the shelter. These layers appear as a clast-supported deposit then subsequently filled in by silty sediments from the Upper Ensemble. A luminescence date obtained from the fine silty fraction provided an age of 64.5 ± 9.2 ka (SU7; BDX16814; Fig. 3b, Table 1), which is discussed in Section 5.2.1.

Deposits in the Upper Ensemble are composed of 2.5-meter-thick loess deposits (Fig. 3a; SU 5-4-3-2) characterized by a) homogenous sedimentary textures with no coarse material inclusions, b) accumulation of secondary carbonates, c) low density of archaeological material, mainly localized in SU5 and 4 (archaeological layer D in Texier et al. 2003). The Upper ensemble was dated from 66.1 ± 5.4 ka (SU4; BDX16813), 66.5 ± 6.8 ka (SU2, 210cm depth; BDX16812) and 57.4 ± 5.4 ka (SU2, 130 cm depth; BDX16811; Fig. 3a, Table 1). SU1 corresponds to the current erosional surface and Ah horizon covering the outer part of the rock shelter sequence.

4.2 – Micromorphology

In order to provide a clearer presentation of sedimentary modes and dynamics of deposition versus pedoclimatic conditions corresponding to syn- or post-depositional climate-related processes, we classified our micromorphological observations in Micromorphological Sedimentary Facies (MSF) and Micromorphological Pedoclimatic Facies (MPF). The facies are presented below, and respective micromorphological descriptions are synthesized in Sup. Mat. Tables A.2, A.3, A.4, A.5.

4.2.1 – Micromorphological Sedimentary Facies (MSF)

MSF-1 Fluvial deposits: Two types of fluvial deposits have been identified: low energy fluvial deposits (MSF-1.a; Fig. 4a) and high energy fluvial deposits (MSF-1.b; Fig. 4a). The first type is characterized by a well-sorted coarse fraction organized in positively graded beds composed of fine sand (80%; 63-100 µm, grain size average 80 µm). The sands comprise sub-angular quartz grains following a coarse monic c/f related distribution pattern and 10-20% of the molassic local parent material. The packing void porosity and the lack of coatings on clastic grains also characterize these facies. The MSF-1.b sub-facies is moderately sorted with rare bedding. The coarse fraction is represented by medium and coarse sand (mean grain size 400 µm; 80%) principally composed of molassic local parent material (70-80%) and quartz grains (20-30%). The c/f related distribution pattern is coarse monic, around a simple packing voids porosity with almost no fine fraction. These coarse-fine laminae typical of Late Glacial floodwater inundation events (recognized in other Mediterranean canyons; Woodward et al., 2001) were produced by La Combette stream floods during periods of enhanced precipitations.

MSF-2 Runoff and colluvium of loess and fine material: Three types of runoff and colluvium deposits have been defined: silty-clay runoff deposit (MSF-2.a; Fig. 7a.2), laminated loess colluvium (MSF-2.b; Fig. 4b; Fig. 7a.1), and non-laminated loess colluvium (MSF-2.c; Fig. 4c; Fig. 7b.1). MSF-2.a refers to massive beds of very well sorted clay and fine silts (3-4 mm thick). The c/f related distribution pattern is fine monic to porphyric. MSF-2.b is very well sorted, organized in sub horizontal, thin laminations (1-2 mm) with fine silty-clay material on the top. This second facies differs from the first one based on a) the enrichment in coarser particles of mica, feldspar, plagioclase, and glauconite; b) sub-rounded coarse material (c/f ratio 70/30); and c) rounded aggregates of fine material. MSF-2.c presents similar characteristics without laminations and is enriched in local molassic rock fragments, often recrystallized and pedorelicts or fragmented clay crusts.

MSF2.b and MSF2.c are characteristic of deposits subject to aeolian transport (Kemp, 1999; Pécsi, 1990; Pye, 1995) combined with syn- and post-depositional transport processes: runoff or colluvial. For these reasons, they are defined as *loess-like sediments* (Cremaschi, 1990). Laminated loess deposits may be the product of short rainfall events that have reworked the original aeolian deposit (Mücher et al., 2010; Mücher and Vreeken, 1981).

MSF-3 Colluvium and Gravity-Induced deposits: This facies gathers remobilized autochthonous parent material due to gravity and mass wasting dynamics. Two sub-facies are defined: coarse molassic slope deposits (MSF-3.a; Fig. 4d) and silty-sandy rock shelter filling (MSF-3.b; Fig. 4e). MSF-3.a is a non-sorted and non-laminated deposit principally composed of medium and coarse sand of local molassic origin (70-80%). The c/f related distribution pattern is coarse monic to chitonic with coarser grains capped or coated by silty clay. The microstructure is pellicular. MSF-3.b is poorly-sorted and non-laminated, composed of angular and sub-angular quartz grains (50-60%) that represent the finest coarse fraction (fine sand and silts), and rounded local molassic parent material (30-40%) that makes up the medium and coarse sand fraction. The fine fraction is well represented (c/f ratio 40/60), the c/f related distribution pattern is porphyric to enaulic, and porosity is organized under compound and complex packing voids. Planar non-accommodated voids often appear in a generally poorly developed granular microstructure.

4.2.2 – Micromorphological Pedological and pedoclimatic Facies (MPF)

MPF-1 Bioturbation facies: These facies was defined based on the degree of bioturbation observed in the thin sections. MPF-1.a represents the total bioturbation of the fabric, characterized by a heavy reorganization of the initial microstructure and the development of a spongy microstructure associated with coated channels (fine soil material on channel walls), chambers, earthworm casts, and micritic hypocoatings (Fig. 7). The latter corresponds to carbonate crystallization around the voids due to evapotranspiration processes (Kemp, 1999; Wieder and Yaalon, 1974). Partial bioturbation is defined by the MPF-1.b facies, recognizable by the initial porosity and microstructure, occasionally reworked by chambers and channels.

MPF-2 Freeze-Thaw features: These pedoclimatic facies includes all features related to ice segregation processes, defined based on their magnitude. Three levels of ice segregation features have been identified: simple ice segregation (MPF-2.a; Fig. 5a, 5b), repeated freeze-thaw cycles (MPF-2.b; Fig. 5c, 5d), and solifluction (MPF-2.c; Fig. 6a- d). These facies are used as indicators of water supply and climatic conditions during cold periods (Van Vliet-Lanoë, 2010, 1985).

Simple ice segregation (MPF-2.a) is recognizable by a planar or lenticular microstructure (Fig. 5a, 5b). Planar voids are non-accommodated to partially accommodated and are often associated with vertical/sub-vertical cracks or star-shaped soil structures. These structures form once the ice melts and are typical of a few freeze-thaw cycles and low water supply periods (Van Vliet-Lanoë et al., 2004). They define an 'isoband fabric' (Dumanski and St. Arnaud, 1966).

The 'bent fabric' is the principal signature of MPF-2.b, which forms during the plastic transformation and migration of some fabric components of the original MPF-2.a patterns. During repeated freeze-thaw cycles, the fine fraction accumulates on top of irregular lenticular peds, while the coarse fraction is progressively englobed (FitzPatrick, 1976; Rowell and Dillon, 1972; Van Vliet-Lanoë, 1976; Fig. 5b, 5c). Settling with displacement structures (Van Vliet-Lanoë, 2010; Fig. 6a), turned silty-clay cappings (20–400 μm), ice blades, and granular microstructure are other markers typical of this facies. MPF-2.b is probably the result of long freeze-thaw cycles during periods of moderate water supply.

MPF-2.c shows a heavy reorganization of the fabric: the coarse fraction is displaced vertically, mechanically fractured (Fig. 5c), and often associated with injection features ("water escape porosity" Phillips et al., 2007). Between the coarser molassic rock fragments, the finer fabric presents a striated b-fabric caused by the reorganization of fine particles under cryogenic and mass movement pressure (Tarnocai and Smith, 1989; van der Meer, 1997; Fig. 5b). Ice blades are bigger than those in the facies MPF-2.b, obliquely oriented and filled by coarse material (Fig. 5a), while silty-clay cappings are rotated (Fig. 5c). The bent fabric forms a well-developed granular microstructure (Fig. 5c), while turned cappings on grains are dissymmetric with a thicker part below the grain. This pedoclimatic facies results from the growing action of ice during multiple freeze-thaw cycles on slopes.

Accepted manuscript version prior to proof-reading.
For the published version see: https://doi.org/10.1016/j.palaeo.2021.110503

MPF-3 Secondary Carbonate features: Two levels of secondary carbonate development have been defined. In the facies MPF-3.a, all the fabric is affected by secondary carbonate precipitation (micritic hypocoatings on voids and micritic coatings on clasts), forming a micritic crystallitic b-fabric (Fig. 7b.2). These features suggest multiple phases of water percolation saturated by carbonates (Monger et al., 1991; Wieder and Yaalon, 1974). MPF-3.b is characterized by rare micritic impregnations in the groundmass and scarce micritic/sparitic coatings/hypo-coatings around voids reflecting occasional carbonate dissolution and re-precipitation processes.

4.2.3 – Micromorphology of La Combette sequence

The Micromorphological facies defined for each SU are synthesized in Fig. 8j. The Lower Ensemble is composed of runoff, slope-wash, and solifluction deposits. SU19 is comprised of runoff (MSF-2.a) and gravity-induced deposits (MSF-3.a), disturbed by cryogenic processes in their upper part (MPF-2.b/.c). SU18 is a gravity-induced slope deposit (MSF-3.a) affected by solifluction (MPF-2.c) and repeated freeze-thaw cycles. A silty-sandy fill (MSF-3.b) and similar pedoclimatic facies (MPF-2.b and MPF-2.c) are recognized throughout SU17.

Sub-ensemble-IIa is characterized alternating low (MSF-1.a) and high (MSF-1.b) energy flow sedimentation with no trace of pedoclimatic syn- or post-depositional features. SU8, composed of coarse molassic slope deposits (MSF-3.a), shows a reduced fluvial accretion and temporary degradation conditions (MPF-2.b).

A shift in sedimentation processes characterizes the upper ensemble. Following the thick torrential sedimentary event (SU7), SU5 is composed of non-laminated loess colluvium (MSF-

2.c) affected by simple ice segregation (MPF-2.a). While SU3 presents traces of laminations (MSF-2.b; Fig. 7a., A.2, A.3), simple ice segregation patterns are still recorded (MPF-2.a) as well as secondary carbonate impregnations (MPF-3.b). SU2, the upper layer of the sequence, is composed of non-laminated loess colluvium (MSF-2.c) highly affected by bioturbation (MPF-1.a) and secondary carbonate precipitation (MPF-3.a; Fig. 7b.1, b.2).

4.3 – Magnetic, Physico-chemical, and sedimentological analyses

4.3.1 - Magnetic Susceptibility

Through the Lower Ensemble, four magnetic peaks were detected with intensities comprised between 27 and 41 SI (Fig. 3b). Peak 1 and peak 2 correspond to SU19 and SU18, while peak 3 corresponds to the interface between SU18 and SU17. Peak 4 marks the boundary between Sub-ensembles-I and -II. These first peaks are measured in areas with high-density archaeological material. High magnetic values could be associated with anthropic heating-induced activity (Brewer, 1964). This hypothesis is confirmed in SU8, where the highest magnetic peak 7 (58 SI) was recorded in a layer composed almost entirely of a diamagnetic clastic fraction (molasses, limestone) and numerous anthropic combustion structures. Peaks 5-6, identified in the laminated fluvial sterile units of Sub-ensemble-II, could correspond to magnetic minerals eroded from oxic soils in the watershed (pedorelicts; Brewer, 1964) (Fig. 4a). In the upper ensemble, the main archaeological layer (SU5) is marked by peak 8, while SU3 shows a slightly higher magnetic signal probably caused by oxide reduction processes (Fig. 3a).

Accepted manuscript version prior to proof-reading.
For the published version see: https://doi.org/10.1016/j.palaeo.2021.110503

4.3.2 - $CaCO_3$ concentration

Total $CaCO_3$ concentration shows a substantial difference between the calcareous clastic composition of the Lower Ensemble (60% < $CaCO_3$ < 70%) and the loessic (mainly quartz) composition of the Upper Ensemble (30% < $CaCO_3$ < 45%), where the total $CaCO_3$ content is mainly the product of secondary carbonates (micromorphological observation; Fig. 8m).

4.3.3 Particle size from laser diffraction

Grain size analysis indicates weakly sorted deposits in Sub-ensemble-I (Fig. 8l). Sub-ensemble-II is marked by an increasing coarse fraction (coarse sand ~8%, medium sand ~20%, fine sand ~70%; Fig. 8l) as well as positive grading. The cumulative curves of the decarbonated SU5-4-3-2 reveal very well sorted silty sands (80-100µm; clay ~10%, silt ~50%, fine sand ~40%), confirming the aeolian origin of this clastic fraction typical of this region (Bosq et al., 2018). Only SU3 shows a slight increase in fine silty and clay material.

4.4 – Heavy-Mineral analysis

4.4.1 - Mineral assemblages

Three mineral assemblages were defined. Based on the existing literature on the Rhône/Durance river basins (Arnaud-Fassetta, 1998; Dubar, 1983; Van Andel, 1955) and the Provence region (Alimen, 1965; Dubar, 1983), two groups of allochthonous heavy minerals

Accepted manuscript version prior to proof-reading.
For the published version see: https://doi.org/10.1016/j.palaeo.2021.110503

were differentiated while our reference samples allowed us to define a local heavy mineral assemblage. **a)** The Massif Central and Rhône group is characterized by the combination of augite, aegyrinic augite, hypersthene, andalusite, basaltic hornblende, and garnet minerals. **b)** The Alpine group comprises glaucophane and epidote in the Durance basin and the southern French Alps, while epidote and hornblende are affiliated with the Isere basin and the northern French Alps. In order to facilitate the interpretation, we have grouped and considered hornblende, glaucophane, actinote, tremolite, chlorite, and choroid as part of the Alpine group. **c)** local molassic heavy minerals are composed of 60–65% garnet, 20–30% resistant minerals (zircon, tourmaline, staurolite), and less than 10% typical alpine or upper Durance valley minerals (hornblende, glaucophane, actinote, tremolite), while epidote/zoisite constitutes 10-15%. Dubar (1983) has shown that molassic rocks from the lower Durance valley are composed of 51% epidote, 40% garnet and resistant minerals, and less than 2% minerals of Alpine origin. This has allowed us to isolate the Luberon local group from the Alpine and the Massif Central /Rhône groups. This is even suggested by the recent geochemical study of loess from the Provence and Rhône regions, which evidenced the enrichment in resistant minerals (quartz, zircon, and Ti oxides; Alpine origin) in Last Glacial Maximum (LGM) aeolian deposits compared to local mineralogical catchment assemblages mainly composed of Ca-rich minerals (Bosq et al., 2020a).

4.4.2 – Evolution of the heavy mineral input in La Combette

As the source of the torrential stream flowing below the rock shelter of La Combette is found in the Luberon Massif and its upstream section is disconnected from the Durance or

Accepted manuscript version prior to proof-reading.
For the published version see: https://doi.org/10.1016/j.palaeo.2021.110503

Rhône river basin (Fig. 1), we suggest that deposits composed of heavy minerals from the Alpine or Massif Central /Rhône groups have undergone at least one aeolian transport cycle. In contrast, the deposits composed principally of local heavy minerals originate from fluviatile or gravity-induced transport from the Aiguebrun watershed.

At the La Combette sequence base, the proportion of local heavy minerals reaches 60-62% (Sub-ensemble-I), with the Alpine input values typically reaching 20–33% (epidote/zoisite ~26%, other alpine minerals ~7%; Fig. 8k). The percentage of the local mineral input increases in Sub-ensemble-II (70-73%), while the alpine one decreases to 7% (epidote/zoisite 4%, alpine minerals 3%). The gradual disappearance of alpine minerals and the increasing local fraction suggests the erosion of local sediments and their transport over short distances during the deposition of Sub-ensemble-II. These results are in accordance with the grain-size analysis and the total $CaCO_3$ concentration analysis.

In the upper Ensemble (starting in SU5), there is a shift in the mineral assemblage with 63% of Alpine group minerals (epidote/zoisite 52%, alpine minerals 11%) and 32% of local minerals (15% garnet, 17% resistant minerals; Fig. 8k). In SU3, the proportion of Alpine group minerals reaches 70%, while the local group decreases to 23%. These results suggest increasing eolian input and decreasing local hydrosedimentary processes. The contribution of the Massif Central /Rhône mineralogical group remains stable around 1% throughout the sequence.

4.5 – Malacofauna study

The malacofauna taxonomic determination is presented in Table 2 and Fig. 7i. A total of 56 individuals were identified, representing 11 species. The low amount of malacological remains does not allow us to provide a solid palaeoecological interpretation. However, some observations can be pointed out and compared to the other complementary proxies.

At the base of the sequence (SU 18 and 17), the combination of *Cepaea sp., Pomatias elegans,* and *Chilostoma squamatimum* suggests a forest or shrubby environment persists until the top of Sub-ensemble-I. In Sub-ensemble-II (SU16 to SU8), the appearance of *Eumphalia strigella* indicates a sub-alpine-like environment characterized by open and shrubby areas. *Eumphalia strigella* is common in the non-pleniglacial Würmian fauna of the Lower Rhône Valley (Bourdier, 1958). The predominance of *Chilostoma squamatimum*, which is characteristic of an open forest environment (Limondin, 1990), is remarkable. In the Languedoc and Provence regions, this species evolves in hairy oak groves (André, 1983), which are considered semi-forested environments. The Upper Ensemble (SU5 to SU2) shows the disappearance of species typical of the forest and the decrease in *Chilostoma squamatimum* (Fig. 8i). The introduction of *Pupilla Triplicata*, *Clausilia parvula*, *Trochoidea geyeri*, and *Abida secale* associations characterizes these upper layers. These species are the most common ones of the Pleniglacial environment in the Provence region, while the substantial absence of *Granaria variabilis* and the reduction of *Chilostoma squamatimum* could indicate a freezing climate with a predominant herbaceous vegetation cover (Magnin, 1991).

5 – Discussion

5.1 – Depositional processes and local palaeoenvironmental conditions

Based on our results and previous studies (Lopez-Saez et al. 1998; Texier et al. 2003; Théry-Parisot and Texier, 2006; Audiard et al., 2019), we can now better describe the sedimentary formation processes, the local hydro-system dynamics in the canyon of La Combette and their link with local palaeoecological and palaeoenvironmental settings (Fig. 8).

5.1.1 – Surface runoff dynamics and temperate/wet conditions

The base of the sedimentary fill of La Combette (SU19) corresponds to laminated runoff deposits. The absence of climate-related pedofeatures indicates the lack of extreme environmental conditions. These deposits were not dated, but a geochronological correlation is proposed in Section 5.2 based on palaeoenvironmental and ecological interpretations.

Palynological data indicate vegetation dominated by *Pinus sylvestris* t., coupled with *Carpinus betulus* t., *Juglans* t., *Castanea, Quercus s.*, and *Pinus sp.*, which reflects a cool environment that is warming up (Fig. 8h; Lopez-Saez et al., 1998). Charcoal data confirm these environmental conditions, with the presence of humid and temperate taxa (*Acer sp.*, *Cornus sp.*, *Ulmus minor*; Fig. 8f; Théry-Parisot and Texier, 2006). This temperate vegetation cover in a wet environment could reflect soil development and palaeolandscape stability in the watershed of La Combette.

5.1.2 – Freeze-thaw syn-sedimentary processes and cold/wet conditions

Within Sub-Ensemble-II, the development of solifluction and freeze-thaw processes indicate shifting environmental conditions between SU19 and SU18, possibly linked to mass wasting dynamics with moderate water availability.

From SU 18, the substantial increase in *Artemisia, Centaurea nigra t.*, and *Papaveraceae* and the general decrease in temperate species suggest a colder environment (Lopez-Saez et al. 1998; Fig. 8h), while malacological data indicate a shrubby vegetation cover (Fig. 8i). Charcoal remains, with a slight decrease in mesophilic species and the appearance of *Salix sp.* (Fig. 8f;

Théry-Parisot and Texier, 2006), point towards a fresh to cold environment. This is also recorded in decreasing $\delta^{13}C$ signal of these charcoal (Fig. 8g; isotopic Phase-I ; Audiard et al., 2018). The slight increase in *Pinus nigra/sylvestris* combined with ice-segregation patterns indicates the persistence of these environmental conditions, with several fluctuations in moisture until the end of Sub-ensemble-I (SU 17; Fig. 8f). Chronologically, the top of this Sub-ensemble (71.9 ± 5.5 ka; 1-sigma) is younger than Sub-ensemble-II (80.1 ± 6.4 ka; 1-sigma), showing an ages inversion. However, the large uncertainties associated with these luminescence dates do not allow us to draw further conclusions.

5.1.2 – Alluvial sedimentation and temperate/wet conditions

Sub-ensemble-II and -III record alluvial sedimentation with the occurrence of medium and high-intensity floods (Fig. 8j), associated with more wet/temperate conditions (SU 16 to 7; Fig.8). The stratigraphy of these two Sub-ensembles corresponds to an inversed erosional stratigraphy. The lower part of the sequence (SU 15 to 10) corresponds to the erosion of fine sediments and ancient soils in the watershed. Indeed, dispersed reddish clay pedorelicts in the deposits (Brewer, 1964; Fig. 4a) suggest the erosion of red soils, which could have formed during a previous stable temperate period, which could correspond to milder interstadials of the MIS5. Above (SU7), coarser deposits correspond to the erosion of the exposed bedrock in the watershed. This specific 'inversed' sequence has already been attested over the southeastern France Mediterranean region and interpreted as evidence of climatic degradation during prominent climatic transitions (Dubar, 1995, 1987, 1983).

Towards the SU16, palynological data indicate warmer conditions with the appearance of *Quercus liex*, *Olea europea*, and *Fraxinus*, the increase in *Juniperus t.* and *Chicorideae*, and

Accepted manuscript version prior to proof-reading.
For the published version see: https://doi.org/10.1016/j.palaeo.2021.110503

the decline of *Pinus sylvestris* (Fig. 8h; Lopez-Saez et al., 1998). This follows the substantial increase in semi-forest malacological taxa and the decrease in $\delta^{13}C$ (Phase-IId, Audiard et al., 2018; Fig. 8g, 8i). Interestingly, one temporary event identified in SU9/SU8 seems to record a short-term hydro-climatic degradation. Indeed, SU8 corresponds to a small stream flow deposit combined with a rapid decrease in semi-forested malacological taxa. These short-term events were also recorded in the high $\delta^{13}C$ values in charcoal (isotopic Phase-IVa; Audiard et al., 2018; Fig. 8g), with cold and dry conditions in SU 9 and higher humidity in SU 8. Relatively to Sub-Ensemble I and the Upper ensemble, however, conditions remain more humid. These sediments are sealed by coarse fluvial-torrential deposits (SU7), marking the end of this phase. Dates range between ~86 ka and 70 ka (Fig. 8e; Table 1).

5.1.3 – Aeolian deposits and cold/dry conditions

The Upper Ensemble (SU5 to SU2) records a substantial sedimentological and environmental shift represented by: a) the appearance of a loess sequence characterized by an allochthonous well-sorted mineral assemblage (Fig. 8j, k, l); b) the re-emergence of discrete freeze-thaw features without prominent soil displacement (Fig. 8j); c) the reduction of pinewood and the development of shrubby riparian vegetation resistant to cold (Fig. 8f; Théry-Parisot and Texier, 2006); d) the reduction of semi-forested malacological taxa (Fig. 8i); e) and the highest values of $\delta^{13}C$ in charcoal, suggesting a more rigorous climate (Fig. 8g; Audiard et al., 2019). This aeolian deposition began around 64.5 ± 9.2 ka (Fig. 8e; Table 1), documenting the installation of glacial and peri-glacial conditions in the region. While the lower part of the ensemble (SU5) indicates typical loess deposition, the presence of clay aggregates from the SU4 (Fig. 8j) indicates the reworking of this original aeolian material and the formation of *loess-*

like sediments (Cremaschi, 1990) (Fig. 7a). Aeolian inputs into and at the southern margin of the Luberon Massif (Fig. 1) could be related to the influence of the Mistral wind regime from the Rhone valley. These hydrosedimentary and palaeoenvironmental conditions are typical of cold and dry environments with low water supply. However, at the end of the aeolian deposition (SU3 and 2), the lack of freeze-thaw pedo-facies with strong $CaCO_3$ secondary concentrations could suggest a slight warming trend (Courty and Vallverdu, 2001).

5.2 – La Combette sequence in a local-to-regional MIS5-MIS4 climatic transition

The combination of pedo-sedimentary and palaeoecological data from the La Combette Sequence allows us to reconstruct local environmental conditions (Fig. 8). The study of Sub-ensembles I, II, and III, indicate alternating warm and cold conditions supported by moderate to a high water supply. Based on new luminescence ages, these conditions are signatures of the hydro-climatic instability of the most recent sub-stages of the Last Interglacial period, between ~90 ka to ~70 ka.

In order to discuss the representativeness of our results at a regional scale, we compared our multiproxy observations with **a**) a close loess-palaeosol sequence recently investigated by Bosq et al. (2020b) in the Rhône valley (Fig. 8d); **b**) two palynological series from the septentrional part of the Rhône basin covering the same period (Fig. 8c; La Grande Pile, Les Echets; Faquette et al., 1999; Klotz et al., 2004; Helmens 2014; Fig. 1); **c**) the MD99-2348 core record from the Rhône deep delta (Fig. 8a, 8b; Sierro et al., 2009)

5.2.1 – The Last Late Interglacial period (~90 - ~70 ka)

The hydrological and palaeoenvironmental signatures recorded at the base of La Combette sequence (Sub-ensemble-I; see 5.1.2), typical of fresh/humid (SU19) to colder (SU18-17) environments, can be correlated to the hydro-climatic variations recorded in the continuous regional archives. Indeed, during the end of MIS5, hydro-climate reconstruction models at La Grande Pile (Fauquette et al. 1999) indicate low but regular precipitation (~500 mm/yr; Fig 8c) and low temperatures. In the Rhône deep delta, this same period is characterized by a relative percentage of temperate/warm foraminifera and low terrigenous inputs (Fig. 8a, 8b; Sierro et al., 2009). We put forward the hypothesis that the lower part of the La Combette sequence belongs to one of the last cold sub-stages at the beginning of the climatic degradation at the end of the MIS5-early MIS4. During this cold period, the rock shelter was highly frequented by Neanderthals as a specialized hunting spot for several expeditions (Texier et al., 2003).

From Sub-ensemble II, a shift of the hydrological regime has been recorded at La Combette with the stepwise increase of fluvial inputs. Regionally, after the cold and relatively low-rainfall period, the Interglacial sub-stage 5.1 (~85 - ~73 ka; Fig. 8) is characterized by higher precipitation values (~800 mm/yr) and temperatures at La Grande Pile (Fauquette et al., 1999; Fig. 8c). In the deep Rhône delta, the gradual increase in temperate/warm foraminiferal species and high $\delta^{18}O$ values on *G. bulloides* confirms the installation of milder conditions (Sierro et al., 2009; Fig. 8a). Sedimentologically, from the same Rhône delta archive, a sandy layer (Fig. 8b) also marks this sub-stage, reflecting the reactivation of the Rhône hydro-system and the landward migration of the coastline (Sierro et al., 2009). Chronologically, this coarser sandy event corresponds to the fluvial-torrential aggradation of the La Combette sequence (Sub-ensemble-II), generally ranged between ~86 ka and ~70 ka (Table 1; Fig. 8). Interestingly, these fluvial deposits contain markers of soil erosion (pedorelicts; Brewer, 1964; Fig. 4), suggesting an ancient soil cover (Interglacial soils) in the watershed of La Combette. In the Rhône watershed, evidence of Bwk red soil pedocomplexes at the Collias sequence was dated between 82.8 ± 7.2 ka and 87.1 ± 6.5 ka (Fig. 8d; Bosq et al., 2020b). There is some coherence in suggesting that these events (hydro-system fluvial reactivation and soil erosion) correspond to more humid conditions at the end of the MIS5 recorded regionally. Over the whole Mediterranean region, several records attested an increase of alluvial activity during this period (Macklin and Woodward, 2009). Indeed, the Last Interglacial – Glacial transition has trigged some significant landscape transformations around the Mediterranean, mainly corresponding to an increase of slope erosion and valley floor aggradation (Macklin and Woodward, 2009).

At La Combette, this humid interval is temporarily interrupted by a short-term episode characterized by reduced fluvial activity, colder environmental conditions, and reoccupation of the shelter (archaeological layer E, SU8; 80.1 ± 6.4 ka; Fig. 8d). This event seems to be absent in continuous continental/marine archives (Figs. 8a, 8b, 8c), underlining the relevance of terrestrial sequences for local to regional palaeoenvironmental reconstructions. Finally, the resumption of fluvial/torrential aggradation (SU7) marks the end of this climatic phase.

In summary, this warmer period recorded at La Combette likely corresponds to the last humid pulses of the MIS5. However, it can even include slight humid oscillations attested at the beginning of the MIS4, until ~70 ka (ex: Ognon complex; Fauquette et al., 1999; Helmens, 2014). However, the low resolution of luminescence ages, as well as the possible occurrence of erosive

Accepted manuscript version prior to proof-reading.
For the published version see: https://doi.org/10.1016/j.palaeo.2021.110503

processes between fluvial events, does not allow us to propose a precise correlation to regional short-term humid oscillations which characterized the end of the MIS5/beginning of MIS4.

5.2.2 – The Early Glacial period (~70-~50 ka)

At La Combette, the first loess deposits have been dated from 66.1 ± 5.4 ka (BDX16813, SU4) in concomitance with steppe-like vegetation. In this cold and arid environment, traces of Neanderthal occupation are scarce apart from archaeological layer D (Texier et al., 2003).

Following our results, the regional palaeoclimatological marine and continental records show a rapid cooling since ~70 ka corresponding to the installation of Würmian glacial conditions (Fig. 8): low $\delta^{18}O$ values in *G. Bulloides,* the reduction of fluvial dynamics (Sierro et al., 2009), the decrease in temperatures and precipitation (<500 mm/yr; La Grande Pile, Fauquette et al., 1999) combined with the spread of steppic species indicate arid conditions (Helmens, 2014). Interestingly, at La Combette, SU3 records a short-term, slightly humid episode (runoff reworking of aeolian material), which possibly corresponds to local hydrological variations. The complete filling of the rock shelter by aeolian deposition marks the end of the sequence during the MIS3 at around 40 ka (cf. Kreutzer et al., 2021; their Fig. 7) with persistent cold and dry climatic patterns until this period. The installation of MIS4-MIS3 loess deposits is even attested in the Rhône valley at La Collias sequence, supporting our results (Fig. 8d; Bosq et al., 2020b).

The interruption of the eolian sediment supply and freeze–thaw processes in the upper layers, accompanied by a marked increase of carbonate weathering, may suggest a slight warming trend (Courty and Vallverdu, 2001). Accordingly, after ~50 ka more temperate

Accepted manuscript version prior to proof-reading.
For the published version see: https://doi.org/10.1016/j.palaeo.2021.110503

conditions were regionally dominant in the Luberon/Lower Durance area, as well as in the Lower Rhône valley (Dubar, 2008; Ollivier et al., 2014, Bosq et al., 2020b), with the development of red and brown soils, likely corresponding to the installation of the Moershoofd-Pile Interstadial until ~40 ka.

6 – Conclusions

Sedimentological, micromorphological, isotopic (charcoal $\delta^{13}C$), and palaeo-ecological (palynology, anthracology, malacology) studies have been combined at the site of La Combette (Luberon massif, western Provence region, France) to provide a new palaeoenvironmental and palaeoclimatological evidence for the MIS5 – MIS4 transition. Our results reveal climatic trends consistent with regional ones, but local data provide new and relevant information:

1) The response to climate change during the last sub-stages of the MIS5 in the Luberon area is characterized by a strong environmental instability, with alternating wet and cold conditions until ~70 ka. The last phase of this period shows a reactivation of the hydrographic system with an increasing erosion, which likely corresponds to the end of the sub-stage MIS5.1 and the onset of the MIS4 (ex: Ognon complex).

2) An important accumulation of cryoturbated loess deposits marks the installation of the glacial period at La Combette. Combined with palaeobotanical data, our results confirm the arid and cold character of the MIS4 and refine the chronology of the loess deposition in the Provence region.

Our results provide new data on the palaeoclimatic context of the Neanderthal settlements in the South of France during the Last Interglacial – Glacial transition, showing the

Accepted manuscript version prior to proof-reading.
For the published version see: https://doi.org/10.1016/j.palaeo.2021.110503

evidence of climatic deterioration characterized by high hydrological and temperature instability followed by cold and dry conditions. They also highlight the necessity to improve the multidisciplinary studies on known continental sequences to constrain further the environmental context of Palaeolithic settlements facing prominent hydro-climatic disruptions.

Acknowledgments

Fieldwork, analyses, and thin section fabrication were funded by the CNRS CEPAM-UMR7264, with the logistic support of P.-J.Texier. We would like to thank L. Meignen and E. Nicoud for their assistance in the field and valuable comments on the manuscript. Thank you also to M. Zanti for his help and support for the grain-size analysis at GEOAZUR-UMR7329. The LaScArBx financed the work of SK. LaScArBx is a research program supported by the ANR (ANR-10-LABX-52).

References

Alimen, H., 1965. Pétrographie des limons de Provence. Bull. Assoc. Fr. Pour Létude Quat. 2, 35–65. https://doi.org/10.3406/quate.1965.979

André, J., 1983. Les peuplements de mollusques terrestres des formations végétales à Quercus pubescens Willd. du Montpelliérais. Premiers résultats. Malacologia 1, 483–488.

Arnaud-Fassetta, G., 1998. Dynamiques fluviales holocènes dans le delta du rhône (thesis). Aix-Marseille 1.

Audiard, B., Thery-Parisot, I., Blasco, T., Mologni, C., Texier, P.-J., Battipaglia, G., 2019. Crossing taxonomic and isotopic approaches in charcoal analyses to reveal past climates. New perspectives in Paleobotany from the Paleolithic Neanderthal dwelling-site of La Combette (Vaucluse, France). Rev. Palaeobot. Palynol. 266, 52–60. https://doi.org/10.1016/j.revpalbo.2019.04.002

Beaulieu, J.-L.D., Reille, M., 1984. A long Upper Pleistocene pollen record from Les Echets, near Lyon, France. Boreas 13, 111–132. https://doi.org/10.1111/j.1502-3885.1984.tb00066.x

Bertran, P., Liard, M., Sitzia, L., Tissoux, H., 2016. A map of Pleistocene aeolian deposits in Western Europe, with special emphasis on France. J. Quat. Sci. 31, e2909. https://doi.org/10.1002/jqs.2909

Bosq, M., Bertran, P., Degeai, J.-P., Kreutzer, S., Queffelec, A., Moine, O., Morin, E., 2018. Last Glacial aeolian landforms and deposits in the Rhône Valley (SE France): Spatial distribution and grain-size characterization. Geomorphology 318, 250–269. https://doi.org/10.1016/j.geomorph.2018.06.010

Bosq, M., Bertran, P., Degeai, J.-P., Queffelec, A., Moine, O., 2020a. Geochemical signature of sources, recycling and weathering in the Last Glacial loess from the Rhône Valley (southeast France) and comparison with other European regions. Aeolian Res. 42, 100561. https://doi.org/10.1016/j.aeolia.2019.100561

Bosq, M., Kreutzer, S., Bertran, P., Degeai, J.-P., Dugas, P., Kadereit, A., Lanos, P., Moine, O., Pfaffner, N., Queffelec, A., Sauer, D., 2020b. Chronostratigraphy of two Late Pleistocene loess-palaeosol sequences in the Rhône Valley (southeast France). Quat. Sci. Rev. 245, 106473. https://doi.org/10.1016/j.quascirev.2020.106473

Bourdier, F., 1958. Le bassin du Rhône au Quaternaire: Géologie et Préhistoire. Fac. Sci. Paris.

Brewer, R., 1964. Fabric and mineral analysis of soils. Wiley.

Bullock, P. (Ed.), 1985. Handbook for soil thin section description. Waine Research Publ, Albrighton.

Buoncristiani, J.-F., Campy, M., 2011. Quaternary Glaciations in the French Alps and Jura, in: Developments in Quaternary Sciences. Elsevier, pp. 117–126. https://doi.org/10.1016/B978-0-444-53447-7.00010-6

Buylaert, J.P., Murray, A.S., Thomsen, K.J., Jain, M., 2009. Testing the potential of an elevated temperature IRSL signal from K-feldspar. Radiat. Meas., Proceedings of the 12th International Conference on Luminescence and Electron Spin Resonance Dating (LED 2008) 44, 560–565. https://doi.org/10.1016/j.radmeas.2009.02.007

Cailleux, A., Tricart, J., 1964. Initiation à l’étude des sables et des galets. Centre de documentation universitaire.

Conrad, G., Onoratini, G., 1997. Le remplissage karstique de la grotte de l’Adaouste et sa genèse (Jouques, B.D.R) [The karstic infilling of Adaouste cave.]. Quaternaire 8, 159–174. https://doi.org/10.3406/quate.1997.1570

Cossart, E., Bourlès, D., Braucher, R., Carcaillet, J., Fort, M., Siame, L., 2011. L’englacement du haut bassin durancien (Alpes françaises du sud) du Dernier Maximum Glaciaire à l’Holocène :

synthèse chronologique. Géomorphologie Relief Process. Environ. 17, 123–142. https://doi.org/10.4000/geomorphologie.9336
Cossart, E., Braucher, R., Fort, M., Bourlès, D.L., Carcaillet, J., 2008. Slope instability in relation to glacial debuttressing in alpine areas (Upper Durance catchment, southeastern France): Evidence from field data and 10Be cosmic ray exposure ages. Geomorphology 95, 3–26. https://doi.org/10.1016/j.geomorph.2006.12.022
Courty, M.-A., Vallverdu, J., 2001. The microstratigraphic record of abrupt climate changes in cave sediments of the Western Mediterranean. Geoarchaeology 16, 467–499. https://doi.org/10.1002/gea.1002
Crégut-Bonnoure, E., 2002. Les ovibovini, caprini et ovini (Mammalia, Artiodactyla, Bovidae, Caprinae) du plio-pléistocène d'Europe occidentale : systématique, évolution et biochronologie (thesis). Lyon 1.
Cremaschi, M., 1990. The loess in Northern and Central Italy: a loess basin between the Alps and the Mediterranean Region. CNR Centro di Studio per la Stratigrafia e la Petrografia delle Alpi Centrali.
Daujeard, C., Fernandes, P., Guadelli, J.-L., Moncel, M.-H., Santagata, C., Raynal, J.-P., 2012. Neanderthal subsistence strategies in Southeastern France between the plains of the Rhone Valley and the mid-mountains of the Massif Central (MIS 7 to MIS 3). Quat. Int. 252, 32–47. https://doi.org/10.1016/j.quaint.2011.01.047
de Beaulieu, J.-L., Reille, M., 1989. The transition from temperate phases to stadials in the long upper Pleistocene sequence from Les Echets (France). Palaeogeogr. Palaeoclimatol. Palaeoecol. 72, 147–159. https://doi.org/10.1016/0031-0182(89)90139-9
de Lumley, H., 1969. Le Paléolithique Inférieur et Moyen du Midi Mediterranéen dans son Cadre Géologique.
de Lumley, H., 1957. Le Moustérien de la Baume des Peyrards (Vaucluse). Bull. Société D'Etude Sci. Nat. Vaucluse 1 1–23.
Defleur, A., Bez, J.-F., Crégut-Bonnoure, E., Desclaux, E., Onoratini, G., Radulescu, C., 1994. Le Niveau Moustérien de la Grotte de l'Adaouste (Jouques, Bouches-du- Rhône). Approche Culturelle et Paléoenvironnement. 39.
Dubar, M., 2008. Découverte d'un fragment osseux de Néanderthalien en 1982 à Forcalquier. Patrim. Pays Forcalquier 11, 18–19.
Dubar, M., 1995. Séquences de transition climatique en domaines fluviatile et karstique dans la région de Nice (A.-M., France), en rapport avec l'eustatisme . [Eustasy-related climatic transition sequences in fluviatile and karstic terrains in the Nice area (Southern France).]. Quaternaire 6, 99–105. https://doi.org/10.3406/quate.1995.2043
Dubar, M., 1987. Age et signification des hautes terrasses des grandes vallées alpines: le cas de la Durance. Géologie Alp. 13, 451–456.
Dubar, M., 1983. Stratigraphie des dépôts du Néogène supérieur et du Pléistocène du bassin de la moyenne Durance ; interprétations géodynamiques et paléogéographiques (Thesis). Université de Provence Aix-Marseille 1.
Dumanski, J., St. Arnaud, R.J., 1966. A micropedological study of eluvial soil horizons. Can. J. Soil Sci. 46, 287–292. https://doi.org/10.4141/cjss66-044
Fauquette, S., Guiot, J., Menut, M., de Beaulieu, J.-L., Reille, M., Guenet, P., 1999. Vegetation and climate since the last interglacial in the Vienne area žFrance/ 17.
FitzPatrick, E.A., 1976. Cryons and Isons. Proc. North Engl. Soils Discuss. Group 11, 31–43.
Gagnepain, J., Gaillard, C., 2003. La grotte de la Baume Bonne (Quinson, Alpes de Haute-Provence): synthèse chronostratigraphique et séquence culturelle d'après les fouilles récentes (1988-1997) 14.
Guillore, P., 1980. Méthode de fabrication mécanique et en série des lames minces. INA P-G, Grignon.

Helmens, K.F., 2014. The Last Interglacial–Glacial cycle (MIS 5–2) re-examined based on long proxy records from central and northern Europe. Quat. Sci. Rev. 86, 115–143. https://doi.org/10.1016/j.quascirev.2013.12.012

Huntley, D.J., Godfrey-Smith, D.I., Thewalt, M.L.W., 1985. Optical dating of sediments. Nature 313, 105–107. https://doi.org/10.1038/313105a0

Jacq, V., Albert, P., Delorme, R., 2005. Le mistral, en 1925 et aujourd'hui: Le mistral- 1280 Quelques aspects des connaissances actuelles. La Météorologie 30–38.

Kemp, R.A., 1999. Micromorphology of loess–paleosol sequences: a record of paleoenvironmental change. CATENA 35, 179–196. https://doi.org/10.1016/S0341-8162(98)00099-X

Klotz, S., Müller, U., Mosbrugger, V., de Beaulieu, J.-L., Reille, M., 2004. Eemian to early Würmian climate dynamics: history and pattern of changes in Central Europe. Palaeogeogr. Palaeoclimatol. Palaeoecol. 211, 107–126. https://doi.org/10.1016/j.palaeo.2004.04.009

Konert, M., Vandenberghe, J., 1997. Comparison of laser grain size analysis with pipette and sieve analysis: a solution for the underestimation of the clay fraction. Sedimentology 44, 523–535. https://doi.org/10.1046/j.1365-3091.1997.d01-38.x

Kreutzer, S., Martin, L., Guérin, G., Tribolo, C., Selva, P., Mercier, N., 2018. Environmental dose rate determination using a passive dosimeter: Techniques and workflow for α-Al_2O_3:C chips. Geochronometria 45, 56–67. https://doi.org/10.1515/geochr-2015-0086

Kreutzer, S., Valladas, H., Texier, P.-J., Moineau, V., Mologni, C., Mercier, N., 2021. The Mousterian loess sequence La Combette (France) and its chronological framework: A re-investigation. Comptes Rendus Palevol. https://doi.org/10.5852/cr-palevol2021v20a14

Lebel, S., Trinkaus, E., 2002. Middle Pleistocene human remains from the Bau de l'Aubesier. J. Hum. Evol. 43, 659–685. https://doi.org/10.1006/jhev.2002.0598

Lebel, S., Trinkaus, E., Faure, M., Fernandez, P., Guerin, C., Richter, D., Mercier, N., Valladas, H., Wagner, G.A., 2001. Comparative morphology and paleobiology of Middle Pleistocene human remains from the Bau de l'Aubesier, Vaucluse, France. Proc. Natl. Acad. Sci. 98, 11097–11102. https://doi.org/10.1073/pnas.181353998

Lemorini, C., 2000. Reconnaître des tactiques d'exploitation du milieu au Paléolithique Moyen: la contribution de l'analyse fonctionnelle : étude fonctionnelle des industries lithiques de Grotta Breuil (Latium, Italie) et de La Combette (Bonnieux, Vaucluse, France)., Archaeopress. ed, Archaeopress. Oxford.

Limondin, L., 1990. Paysages et climats quaternaires par les mollusques continentaux. Université Paris 1 Panthéon Sorbonne, Paris.

López-Sáez, J.A., Texier, P.J., Thi Mai, B., 1998. Paléoenvironment durant le Pleistocene Supérieur en Vaucluse: analyse palynologique des couches inférieures de l´abri de la Combette (Bonnieux, Vaucluse, France). Trab. Prehist. 55, 151–162. https://doi.org/10.3989/tp.1998.v55.i2.308

Macklin, M., Woodward, J., 2009. River Systems and Environmental Change, in: The Physical Geography of the Mediterranean. Oxford University Press. https://doi.org/10.1093/oso/9780199268030.003.0023

Magnin, F., 1991. Mollusques continentaux et histoire quaternaire des milieux méditerranéens (sud-est de la France, Catalogne) (thesis). Aix-Marseille 2.

Moncel, M., Daujeard, C., Cregut-Bonnoure, É., Boulbes, N., Puaud, S., Debard, É., Bailon, S., Desclaux, E., Escude, É., Roger, T., Dubar, M., 2010. Nouvelles données sur les occupations humaines du début du Pléistocène supérieur de la moyenne vallée du Rhône (France). Les sites de l'abri des pêcheurs, de la Baume Flandin, de l'Abri du Maras et de la grotte du Figuier (Ardèche). Quaternaire 385–411. https://doi.org/10.4000/quaternaire.9212

Moncel, M.-H., Bahain, J.-J., Falguères, C., Patou-Mathis, M., Rousseau, L., Valladas, H., Auguste, P., Ayliffe, L., Bocherens, H., Bouteaux, A., Condemi, S., Crégut-Bonnoure, E., Crépin, L., Daschek, E., Debard, E., Desclaux, E., Dubar, M., Dubois, J.-M., El Hazzazi, N., Fernandes, P., Froget, L., Chacón Navarro, M.-G., Joron, J.-L., Julien, M.-A., Lamarque, F., Liouville, M., Mallye, J.-B., Masaoudi, H., Mercier, N., Pautret-Homerville, C., Péan, S., Reyss, J.-L., Villette, P., 2008. Le site de Payre. Occupations humaines dans la vallée du Rhône à la fin du Pléistocène moyen et au début du Pléistocène supérieur. Société Préhistorique Française.

Monger, H.C., Daugherty, L.A., Gile, L.H., 1991. A Microscopic Examination of Pedogenic Calcite in an Aridisol of Southern New Mexico. Occur. Charact. Genes. Carbonate Gypsum Silica Accumul. Soils sssaspecialpubl, 37–60. https://doi.org/10.2136/sssaspecpub26.c3

Mücher, H., van Steijn, H., Kwaad, F., 2010. Chapter 2 - Colluvial and Mass Wasting Deposits, in: Stoops, G., Marcelino, V., Mees, F. (Eds.), Interpretation of Micromorphological Features of Soils and Regoliths (Second Edition). Elsevier, pp. 21–36. https://doi.org/10.1016/B978-0-444-63522-8.00002-4

Mücher, H.J., Vreeken, W.J., 1981. (Re)deposition of loess in southern Limbourg, The Netherlands. 2. Micromorphology of the lower silt loam complex and comparison with deposits produced under laboratory conditions. Earth Surf. Process. Landf. 6, 355–363. https://doi.org/10.1002/esp.3290060314

Murray, A.S., Wintle, A.G., 2000. Luminescence dating of quartz using an improved single-aliquot regenerative-dose protocol. Radiat. Meas. 32, 57–73. https://doi.org/10.1016/S1350-4487(99)00253-X

Ollivier, V., Magnin, F., Guendon, J.L., Miramont, C., 2014. Regards sur les dynamiques paysagères du Pléistocène Supérieur du Luberon et de Basse Provence (SIM 3 et SIM 2, France). Quaternaire 91–111. https://doi.org/10.4000/quaternaire.7002

Parfenoff, A., Pomerol, C., Torenq, J., 1970. Les Minéraux en grains : méthodes d'étude et détermination. Masson. Paris.

Pécsi, M., 1990. Loess is not just the accumulation of dust. Quat. Int. 7–8, 1–21. https://doi.org/10.1016/1040-6182(90)90034-2

Phillips, E., Merritt, J., Auton, C., Golledge, N., 2007. Microstructures in subglacial and proglacial sediments: understanding faults, folds and fabrics, and the influence of water on the style of deformation. Quat. Sci. Rev. 26, 1499–1528. https://doi.org/10.1016/j.quascirev.2007.03.007

Preusser, F., Degering, D., Fuchs, M., Hilgers, A., Kadereit, A., Klasen, N., Krbetschek, M., Richter, D., Spencer, J.Q.G., 2008. Luminescence dating: basics, methods and applications. EG Quat. Sci. J. 57, 95–149. https://doi.org/10.3285/eg.57.1-2.5

Pye, K., 1995. The nature, origin and accumulation of loess. Quat. Sci. Rev. 15.

Reille, M., Guiot, J., de Beaulieu, J.-L., 1992. The Montaigu Event: An Abrupt Climatic Change During the Early Wurm in Europe, in: Kukla, G.J., Went, E. (Eds.), Start of a Glacial. Springer Berlin Heidelberg, Berlin, Heidelberg, pp. 85–95. https://doi.org/10.1007/978-3-642-76954-2_7

Richter, D., Richter, A., Dornich, K., 2015. Lexsyg smart — a luminescence detection system for dosimetry, material research and dating application. Geochronometria 42. https://doi.org/10.1515/geochr-2015-0022

Rowell, D.L., Dillon, P.J., 1972. Migration and Aggregation of Na and Ca Clays by the Freezing of Dispersed and Flocculated Suspensions. J. Soil Sci. 23, 442–447. https://doi.org/10.1111/j.1365-2389.1972.tb01675.x

Salonen, J.S., Helmens, K.F., Brendryen, J., Kuosmanen, N., Väliranta, M., Goring, S., Korpela, M., Kylander, M., Philip, A., Plikk, A., Renssen, H., Luoto, M., 2018. Abrupt high-latitude climate events and decoupled seasonal trends during the Eemian. Nat. Commun. 9. https://doi.org/10.1038/s41467-018-05314-1

Saos, T., Djerrab, A., Defleur, A., 2014. Etude stratigraphique, sédimentologique et magnétique des dépôts pléistocène moyen et supérieur de la Baume Moula-Quercy (Soyons, Ardèche). Quaternaire 237–251. https://doi.org/10.4000/quaternaire.7065

Seret, G., Dricot, E., Wansard, G., 1990. Evidence for an early glacial maximum in the French Vosges during the last glacial cycle. Nature 346, 453–456. https://doi.org/10.1038/346453a0

Sierro, F.J., Andersen, N., Bassetti, M.A., Berné, S., Canals, M., Curtis, J.H., Dennielou, B., Flores, J.A., Frigola, J., Gonzalez-Mora, B., Grimalt, J.O., Hodell, D.A., Jouet, G., Pérez-Folgado, M.,

Schneider, R., 2009. Phase relationship between sea level and abrupt climate change. Quat. Sci. Rev. 28, 2867–2881. https://doi.org/10.1016/j.quascirev.2009.07.019
Slimak, L., Lewis, J.E., Crégut-Bonnoure, E., Metz, L., Ollivier, V., André, P., Chrzavzez, J., Giraud, Y., Jeannet, M., Magnin, F., 2010. Le Grand Abri aux Puces, a Mousterian site from the Last Interglacial: paleogeography, paleoenvironment, and new excavation results. J. Archaeol. Sci. 37, 2747–2761. https://doi.org/10.1016/j.jas.2010.06.010
Stoops, G., 2003. Guidelines for Analysis and Description of Soil and Regolith Thin Sections.
Tarnocai, C., Smith, C.A.S., 1989. Micromorphology and development of some central Yukon paleosols, Canada. Geoderma 45, 145–162. https://doi.org/10.1016/0016-7061(89)90047-5
Texier, P.-J., Brugal, J.-P., Desclaux, E., Lemorini, C., Sâez, J.A.L., Thery, I., Wilson, L., 2003. La Combette (Bonnieux, Vaucluse, France): a Mousterian sequence in the Luberon mountain chain, between the plains of the Durance and Calavon rivers 15.
Théry-Parisot, I., Texier, P.-J., 2006. La collecte du bois de feu dans le site moustérien de la Combette (Bonnieux, Vaucluse, France) : implications paléo-économiques et paléo-écologiques. Approche morphométrique des charbons de bois). Bull. Société Préhistorique Fr. 103, 453–463. https://doi.org/10.3406/bspf.2006.13466
Thomsen, K.J., Murray, A.S., Jain, M., Bøtter-Jensen, L., 2008. Laboratory fading rates of various luminescence signals from feldspar-rich sediment extracts. Radiat. Meas. 43, 1474–1486. https://doi.org/10.1016/j.radmeas.2008.06.002
Tiercelin, J.-J., 1977. Fronts glaciaires d'âge Würmien dans les environs du Poët, vallée de la Durance. Géologie Méditerranéenne 4, 307–312. https://doi.org/10.3406/geolm.1977.1012
Van Andel, T.H., 1955. Sediments of the Rhone delta : sources and deposition of heavy minerals. Geol. Ser. Deel 15, 502–555.
van der Meer, J.J.M., 1997. Particle and aggregate mobility in till: Microscopic evidence of subglacial processes. Quat. Sci. Rev. 16, 827–831. https://doi.org/10.1016/S0277-3791(97)00052-8
Van Vliet-Lanoë, B., 2010. Chapter 20 - Frost Action, in: Interpretation of Micromorphological Features of Soils and Regoliths (Second Edition). Elsevier, pp. 575–603. https://doi.org/10.1016/B978-0-444-63522-8.00020-6
Van Vliet-Lanoë, B., 1985. Frost Effects on Soil, in: Soils and Quaternary Landscape Evolution. Boardman J., pp. 117–158.
Van Vliet-Lanoë, B., 1976. Traces de segrégations de glace associées aux sols et phénomènes périglaciaires fossiles. Biul. Peryglac. 26, 41–54.
Van Vliet-Lanoë, B., Fox, C.A., Gubin, S.V., 2004. Micromorphology of Cryosols, in: Kimble, J.M. (Ed.), Cryosols: Permafrost-Affected Soils. Springer Berlin Heidelberg, Berlin, Heidelberg, pp. 365–390. https://doi.org/10.1007/978-3-662-06429-0_18
Walther, R., 1995. Elektronen-Spin-Resonanz-Datierung an Silikaten. Grundlagen, Systematik und Anwendung am Beispiel von Quarzen und Feuerstein. University of Heidelberg.
Wieder, M., Yaalon, D.H., 1974. Effect of matrix composition on carbonate nodule crystallization. Geoderma 11, 95–121. https://doi.org/10.1016/0016-7061(74)90010-X
Willmes, M., Grün, R., Douka, K., Michel, V., Armstrong, R.A., Benson, A., Crégut-Bonnoure, E., Desclaux, E., Fang, F., Kinsley, L., Saos, T., Defleur, A.R., 2016. A comprehensive chronology of the Neanderthal site Moula-Guercy, Ardèche, France. J. Archaeol. Sci. Rep. 9, 309–319. https://doi.org/10.1016/j.jasrep.2016.08.003
Wilson, L., Browne, C.L., Texier, P.-J., 2018. Provisioning on the periphery: Middle Palaeolithic raw material supply strategies on the outer edge of a territory at La Combette (France). J. Archaeol. Sci. Rep. 21, 87–98. https://doi.org/10.1016/j.jasrep.2018.07.001
Woillard, G.M., Mook, W.G., 1982. Carbon-14 Dates at Grande Pile: correlation of land and sea chronologies. Science 159–161.
Woodward, J.C., Hamlin, R.H.B., Macklin, M.G., Karkanas, P., Kotjabopoulou, E., 2001. Quantitative sourcing of slackwater deposits at Boila rockshelter: A record of lateglacial flooding and

Paleolithic settlement in the Pindus Mountains, Northwest Greece. Geoarchaeology 16, 501–536. https://doi.org/10.1002/gea.1003

Tables

SAMPLE	Depth North section	SU	Archaeological layer	$\dot{D}_{total}$ [Gy kyr^{-1}]	D_e [Gy]	*Age* [ka]
BDX16811	130 cm	2	A	2.0 ± 0.1	114.9 ± 7.8	57.4 ± 5.4
BDX16812	210 cm	2	B/C	1.8 ± 0.1	119.5 ± 8.9	66.5 ± 6.8
BDX16813	330 cm	4	D	1.8 ± 0.1	117.2 ± 4.8	66.1 ± 5.4
BDX16814	440 cm	7	/	1.9 ± 0.1	125.2 ± 15.6	64.5 ± 9.2
BDX16815	510 cm	8	E	1.5 ± 0.1	118.8 ± 3.5	80.1 ± 6.4
BDX16816	520 cm	17	F/G	1.8 ± 0.1	126.4 ± 3.9	71.9 ± 5.5

Table 1: Equivalent doses, environmental dose rates and luminescence ages on quartz after (Kreutzer et al., 2021).

SU	Archaeological layer	Depth (North section, cm)	*Pomatias elegans*	*Granaria variabilis*	*Chilostoma squamatimum*	*Clausilia Parvula*	*Abida secale*	*Trochoidea Geyeri*	*Cepaea sp.*	*Vallonia costata*	*Eumphalia strigella*	*Oxychilus*	*Limacelles*
2	B/C	225-230			1	1							
2	B/C	230-235			1								
2	B/C	235-240			1								2
2	B/C	240-245			1	1	1						
4	D	330-335			1								
4	D	335-340	1		1								

5	D	340-345			1								
5	D	345-350		1	1								
5	D	350-355		1	1								1
7		410-415	1										
7		415-420			1		1						
8	E	435-440			1								
8	E	440-445			3								
8	E	445-450			3	2							
8	E	450-455			2	1						1	
8	E	455-460			1						1		
17	F/G	490-495	1		1								
17	F/G	495-500	1	2	1								
17	F/G	500-505	1		3			1		1			
18	F/G	505-510	1		1	1			1	1			
Tot			**6**	**4**	**26**	**6**	**4**	**3**	**1**	**2**	**1**	**1**	**3**

Table 2: Malacological determination of archaeological layers of La Combette

Captions

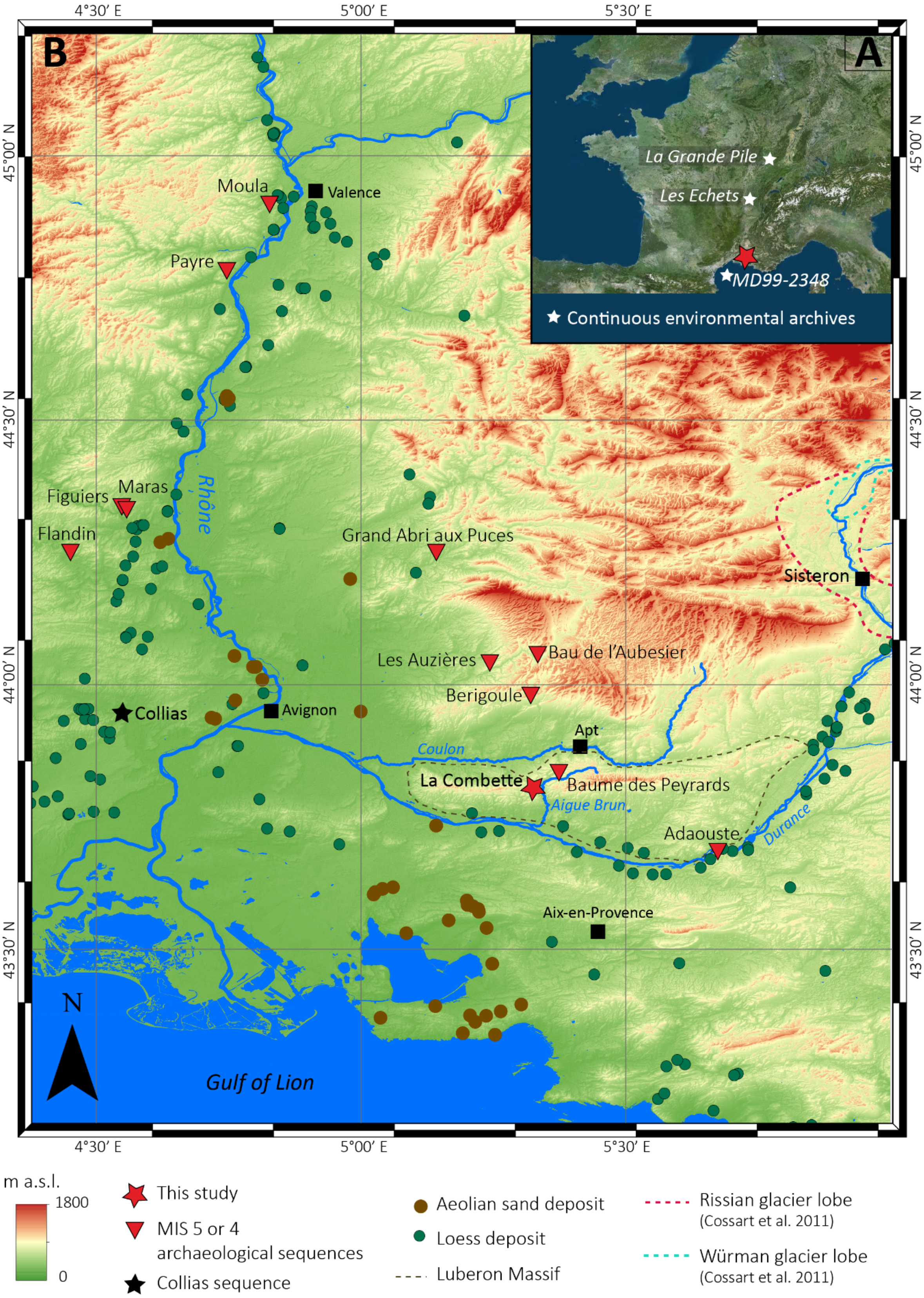

4°30′ E
5°00′ E
5°30′ E
45°00′ N
44°30′ N
44°00′ N
43°30′ N
B
A
La Grande Pile
Les Echets
MD99-2348
Continuous environmental archives
Moula
Valence
Payre
Figuiers
Maras
Flandin
Rhône
Grand Abri aux Puces
Sisteron
Les Auzières
Bau de l'Aubesier
Berigoule
Collias
Avignon
Apt
Coulon
La Combette
Baume des Peyrards
Aigue Brun
Adaouste
Durance
Aix-en-Provence
N
Gulf of Lion
m a.s.l.
1800
0
This study
MIS 5 or 4 archaeological sequences
Collias sequence
Aeolian sand deposit
Loess deposit
Luberon Massif
Rissian glacier lobe (Cossart et al. 2011)
Würman glacier lobe (Cossart et al. 2011)

924

Figure 1: **a)** Geographic location of the regional study area and other important regional palaeoclimate records (white stars): 'La Grande Pile' (Fauquette et al., 1999; Helmens, 2014; Seret et al., 1990; Woillard and Mook, 1982), 'Les Echets' (Beaulieu and Reille, 1984; de Beaulieu and Reille, 1989), MD99-2348 core (Sierro et al., 2009); **b)** 'La Combette' rock shelter (red star), the Collias sequence (black star; Bosq et al., 2020b), the other MIS5/4 sequences discussed in this study (reversed red triangles), the main towns (black squares); the aeolian sand and loess deposits (brown and green dots; Bertran et al., 2016; Bosq et al., 2020, 2018), the Luberon Massif area (brown dotted line), the Rissian and Würmian (red and blue dotted lines respectively) glacier lobe extents (Buoncristiani and Campy, 2011; Cossart et al., 2011, 2008).

Accepted manuscript version prior to proof-reading.
For the published version see: https://doi.org/10.1016/j.palaeo.2021.110503

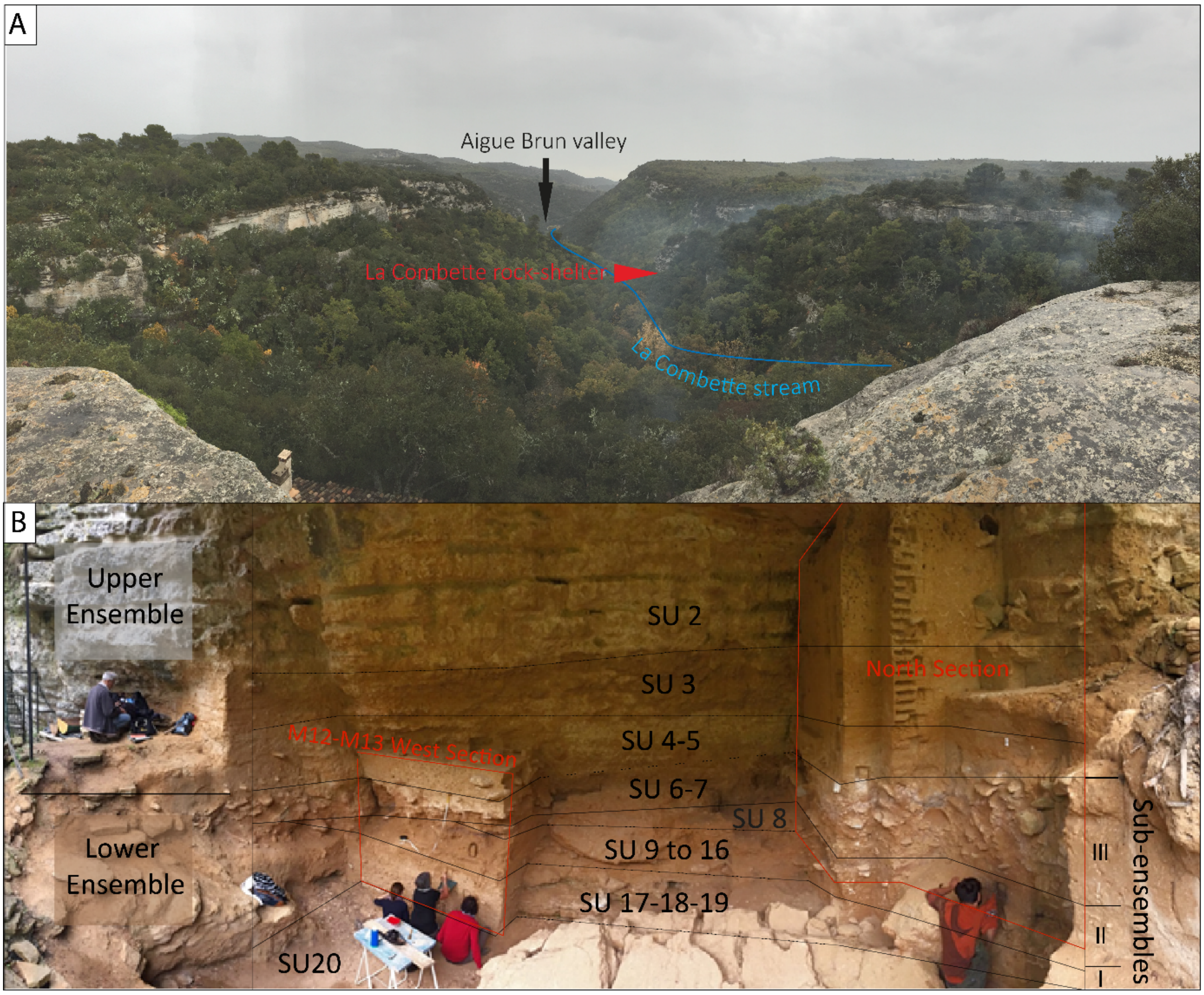

Figure 2: **a)** Picture of La Combette stream landscape with the rock shelter location; **b)** La Combette sequence picture with the location of SU and sampled sections.

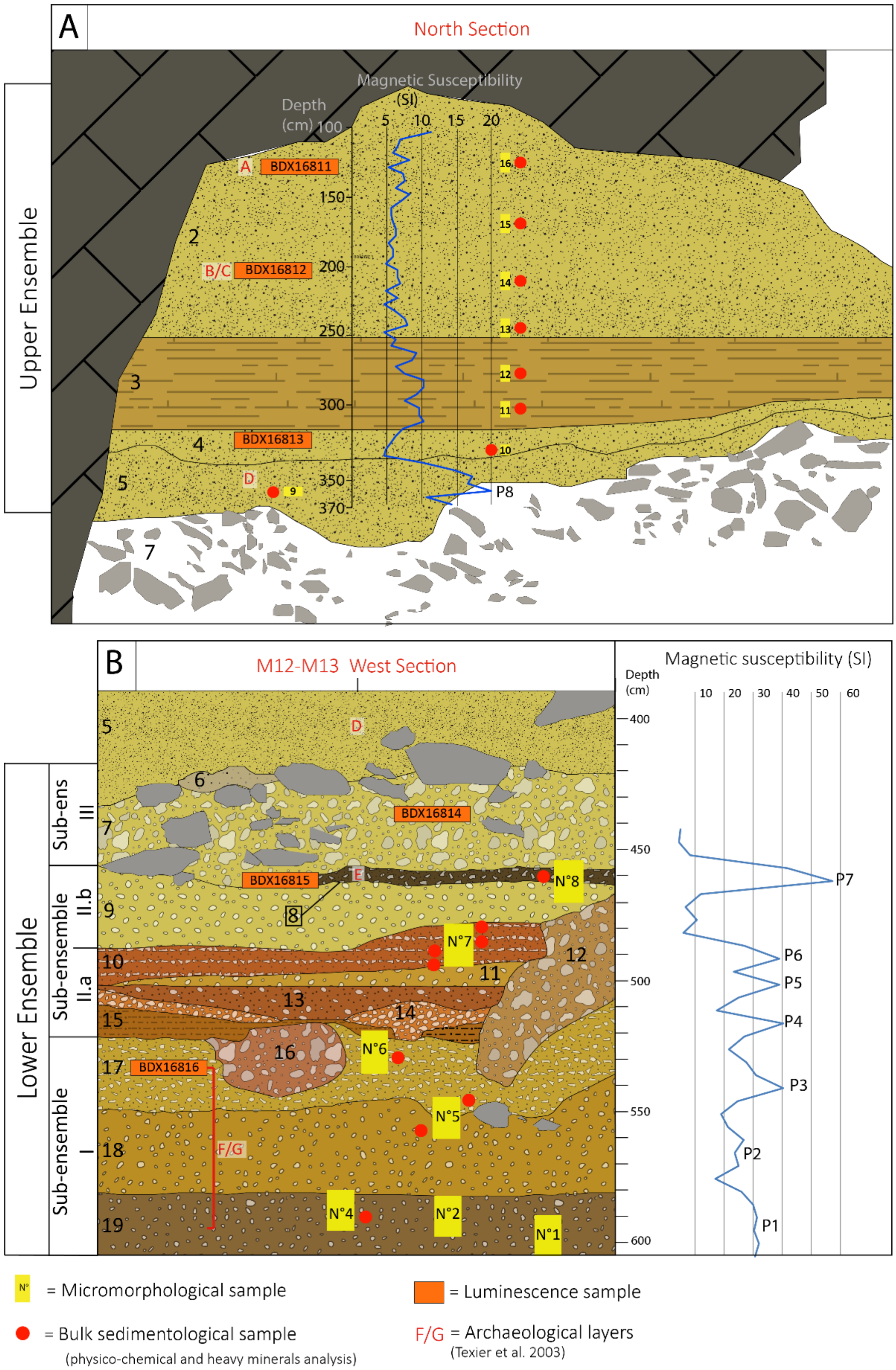

Figure 3: **a)** Upper and **b)** Lower sedimentary Ensembles stratigraphy (SU and archaeological layers), with location of luminescence samples (orange squares), micromorphological (yellow squares), sedimentological samples (red dots) and magnetic susceptibility results (blue curve-line).

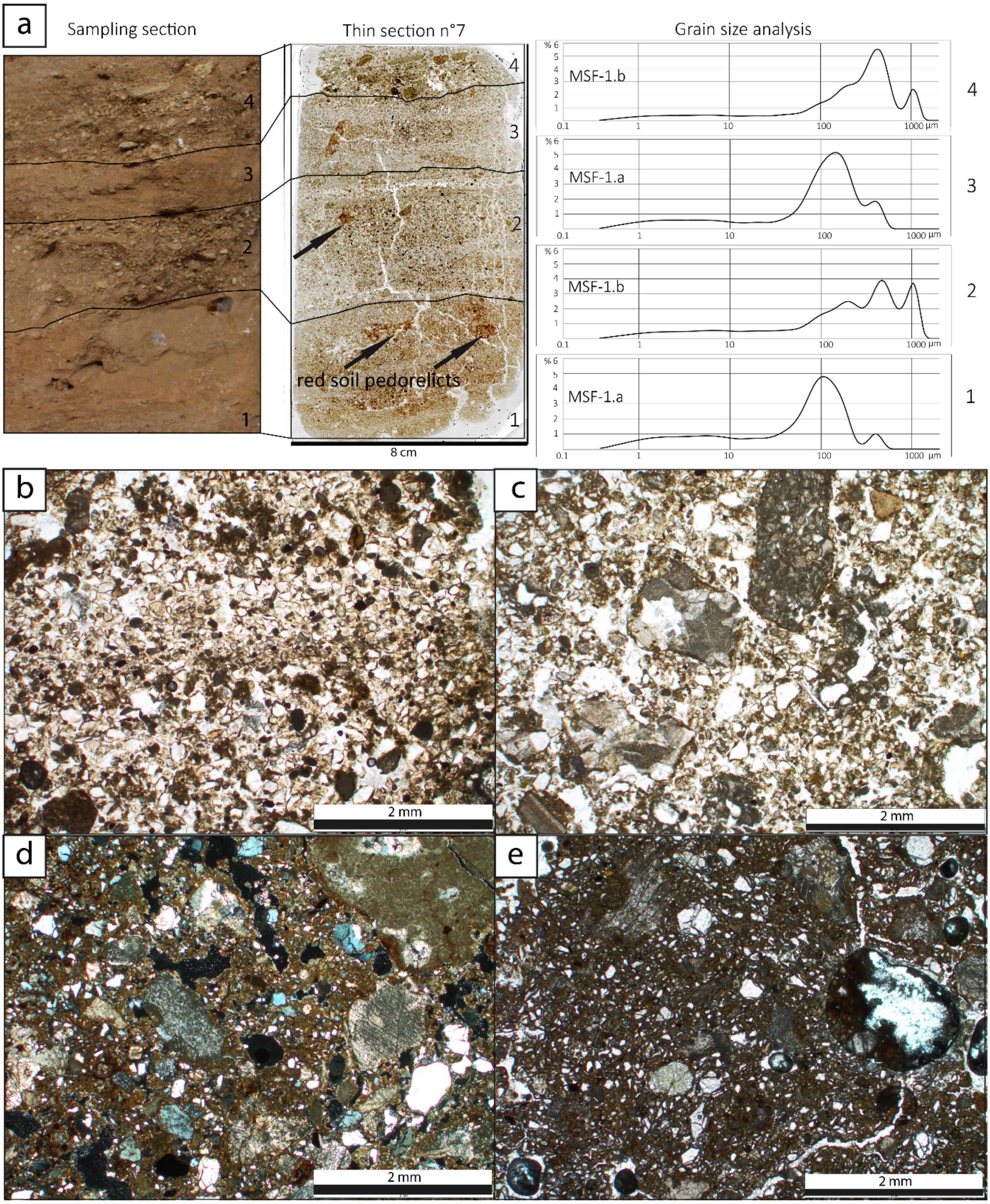

Figure 4: **a)** sediment picture, thin section n°7 scan (PPL) with indicated the red soil pedorelicts (black arrows) and grain size Gaussian distribution of MSF-1.a and MSF-1.b facies; **b)** Microphotography of the MSF-2.b facies (PPL); **c)** Microphotography of the MSF-2.c facies (PPL); **d)** Microphotography of the MSF-3.a facies (XPL); **e)** Microphotography of the MSF-3.b facies (PPL).

954 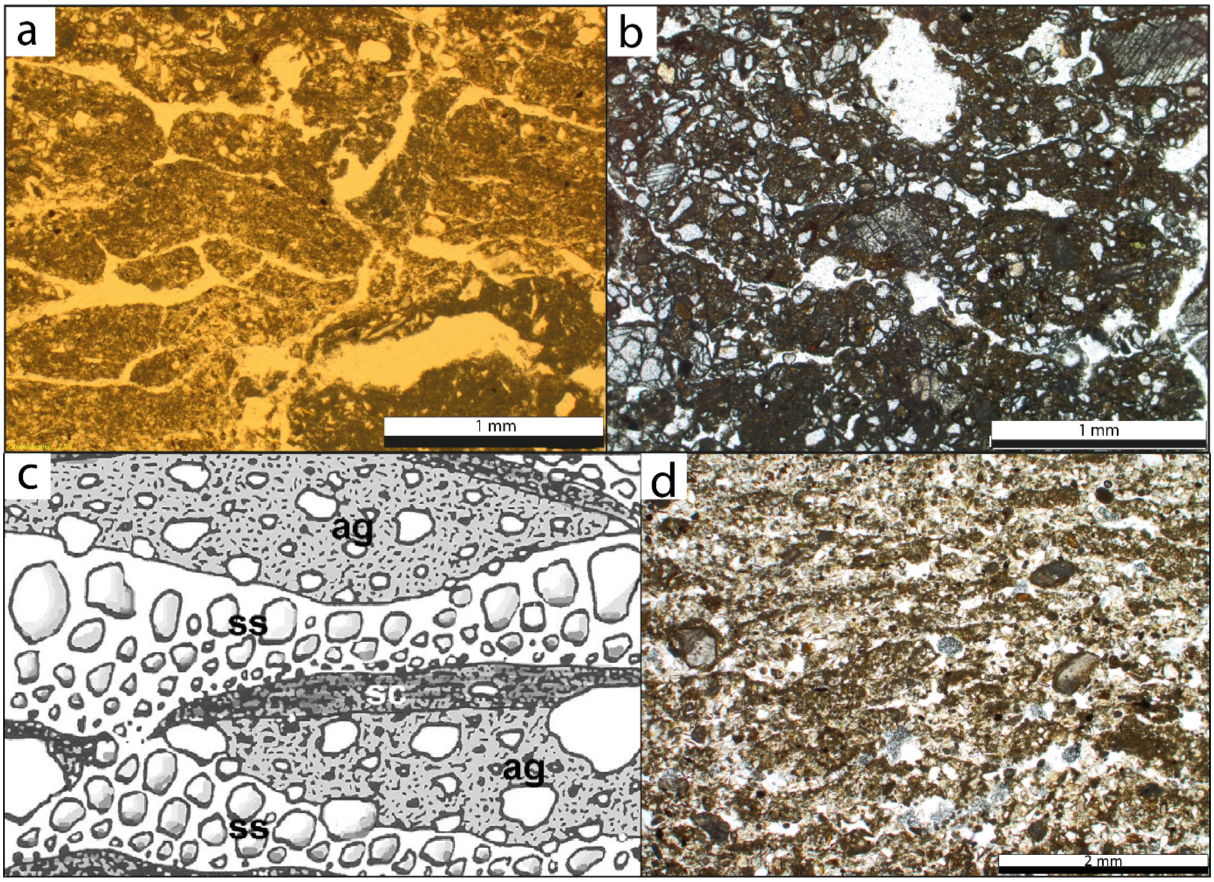

955 **Figure 5**: Microphotographs of pedoclimatic markers belonging to the MPF-2a and MPF-2b facies **a)** Simple ice
956 segregation MPF-2.a facies in a runoff deposit (MSF-2.a; (PPL); **b)** simple ice segregation MPF-2.a facies in a silty-
957 sandy rock shelter filling (MSF-3.b facies PPL); **c)** MPF-2.b facies: well developed 'banded fabric': (ss) sorted sand
958 grains with inverted grading, (sc) layered silt cappings, (ag) lenticular aggregate, after Van Vliet-Lanoë (2010); **d)**
959 MPF-2.b facies: 'bended fabric' from SU3 (thin section n°11; PPL).

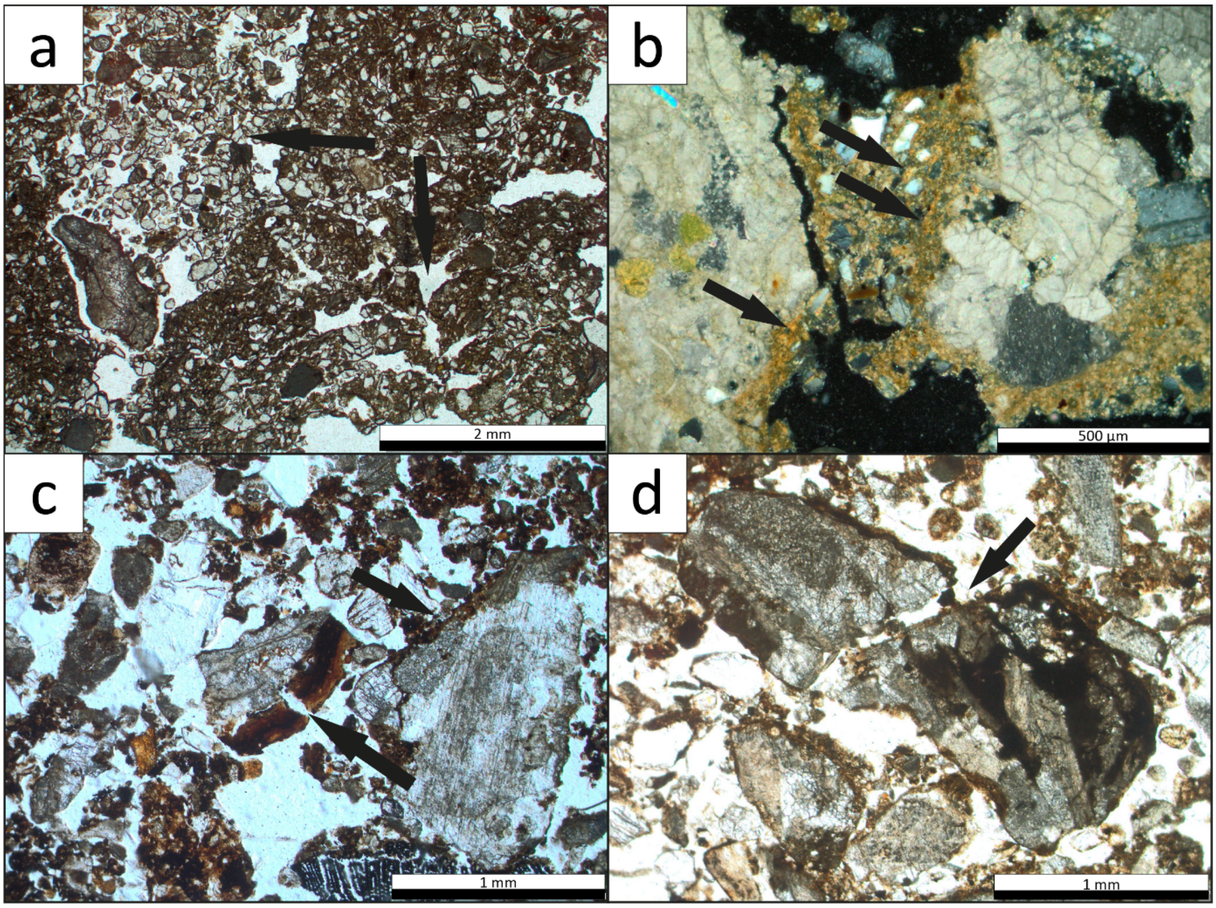

Figure 6: **:** Microphotographs of pedoclimatic markers belonging to the MPF-2c facies **a)** MPF-2.c facies: black arrows indicate the ice blade fine-sand-filling and the settling with displacement microstructure (PPL); **b)** MPF-2.c facies: black arrows indicate the strial b-fabric between two molassic coarse fragments (XPL); **c)** MPF-2.c facies: black arrows indicate the fissured and rotated clayey-silty cappings in a well-developed granular microstructure (PPL); **d)** MPF-2.c facies: black arrows indicate the mechanical fragmented molassic very coarse sand grain (PPL).

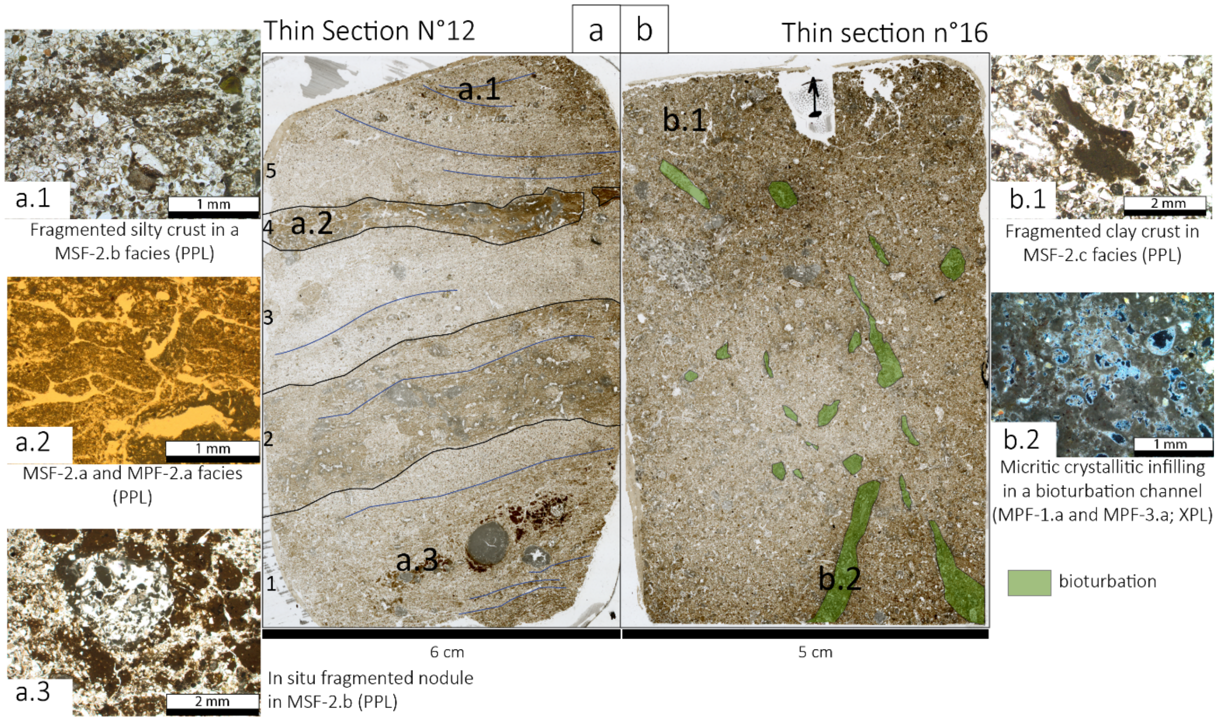

Figure 7: **a)** scan of thin section n°12 (SU3; PPL), alternating silty-clay runoff (MSF-2.a, micro-SU 2, 4) and laminated loess colluvium (MSF-2.b, micro-US1, 3, 5): **a.1)** Microphotograph of a fragmented clay-silty crust - MSF-2.b facies (PPL); **a.2)** Microphotograph of facies MSF-2.a and MPF-2a (PPL); **a.3)** Microphotograph of an in situ fragmented nodule - MSF-2.b facies. **b)** scan of thin section n° 16 (SU2; PPL): **b.1)** Microphotograph of a fragmented clay crust- MSF-2.c facies (PPL); **b.2)** Microphotograph of a micritic crystallite infillings in a bioturbation channel (MPF-1.a and MPF-3.a; XPL).

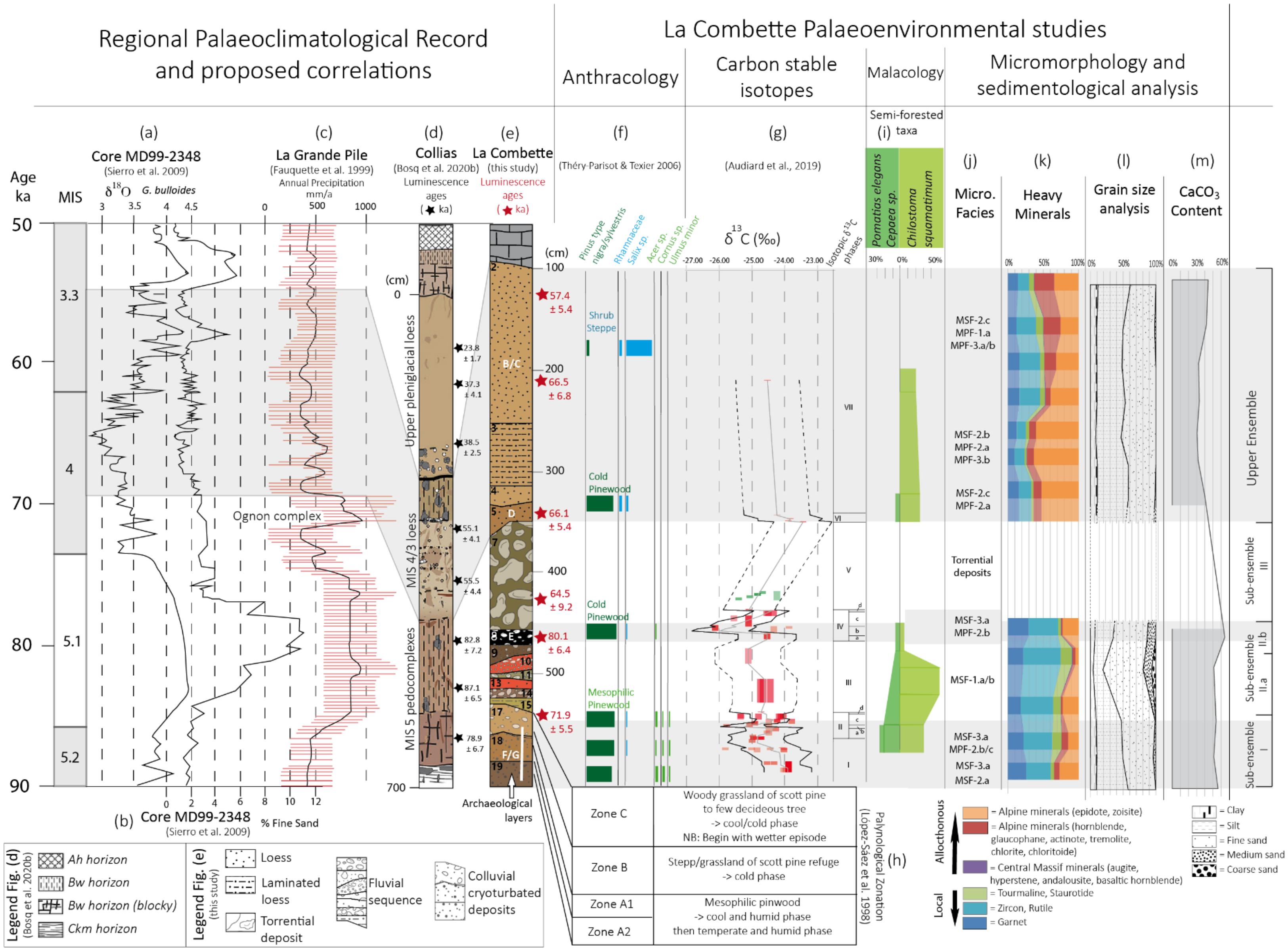

Regional Palaeoclimatological Record and proposed correlations
La Combette Palaeoenvironmental studies
Anthracology
Carbon stable isotopes
Malacology
Micromorphology and sedimentological analysis
(a) Core MD99-2348 (Sierro et al. 2009)
(c) La Grande Pile (Fauquette et al. 1999) Annual Precipitation mm/a
(d) Collias (Bosq et al. 2020b) Luminescence ages (★ ka)
(e) La Combette (this study) Luminescence ages (★ ka)
(f) (Théry-Parisot & Texier 2006)
(g) (Audiard et al., 2019)
(i) Semi-forested taxa
(j) Micro. Facies
(k) Heavy Minerals
(l) Grain size analysis
(m) CaCO3 Content
Age ka
MIS
(b) Core MD99-2348 (Sierro et al. 2009)
% Fine Sand
Ognon complex
Upper pleniglacial loess
MIS 4/3 loess
MIS 5 pedocomplexes
Archaeological layers
Shrub Steppe
Cold Pinewood
Mesophilic Pinewood
Upper Ensemble
Sub-ensemble III
Sub-ensemble II.a
Sub-ensemble II.b
Sub-ensemble I
Torrential deposits
Zone C
Woody grassland of scott pine to few decideous tree -> cool/cold phase NB: Begin with wetter episode
Zone B
Stepp/grassland of scott pine refuge -> cold phase
Zone A1
Mesophilic pinwood -> cool and humid phase then temperate and humid phase
Zone A2
(h) Palynological Zonation (López-Sáez et al. 1998)
Legend Fig. (d) (Bosq et al. 2020b)
Ah horizon
Bw horizon
Bw horizon (blocky)
Ckm horizon
Legend Fig. (e) (this study)
Loess
Laminated loess
Torrential deposit
Fluvial sequence
Colluvial cryoturbated deposits
Allochthonous
Local
= Alpine minerals (epidote, zoisite)
= Alpine minerals (hornblende, glaucophane, actinote, tremolite, chlorite, chloritoide)
= Central Massif minerals (augite, hyperstene, andalousite, basaltic hornblende)
= Tourmaline, Staurotide
= Zircon, Rutile
= Garnet
= Clay
= Silt
= Fine sand
= Medium sand
= Coarse sand

Figure 8: La Combette results compared to the regional continuous palaeoclimatic records: **a)** $\delta^{18}O$ on G. bulloides and **b)** fine sand (%) curves from the MD99-2348 core (Sierro et al., 2009); **c)** annual precipitations (mm/a) based on the sequence of La Grande Pile (Fauquette et al., 1999); **d)** Stratigraphy of the Collias section (Bosq et al., 2020b), with the location of the luminescence samples (black stars); **e)** stratigraphy of La Combette section with the location of luminescence samples (red stars); **f)** anthracological results (Théry-Parisot and Texier, 2006; Audiard et al., 2019); **g)** $\delta^{13}C$ on charcoal results (Audiard et al., 2019); **h)** palynological results on the La Combette sequence (Lopéz-Saéz et al., 1998);**i)** malacological results; **j)** micromorphological facies defined along the sequence of La Combette (this manuscript); **k)** heavy minerals analysis results (this manuscript); **l)** grain size analysis results (this manuscript); **m)** calcium carbonate concentration analysis results (this manuscript).

Accepted manuscript version prior to proof-reading.
For the published version see: https://doi.org/10.1016/j.palaeo.2021.110503

Accepted manuscript version prior to proof-reading.
For the published version see: https://doi.org/10.1016/j.palaeo.2021.110503